

Dual role of B7 costimulation in obesity-related non-alcoholic steatohepatitis (NASH) and metabolic dysregulation

Antonios Chatzigeorgiou^{1,2,3,4,*}, Kyoung-Jin Chung^{1,5,*}, Ruben Garcia-Martin¹, Vasileia-Ismini Alexaki¹, Anne Klotzsche-von Ameln^{1,5}, Julia Phieler^{1,4}, David Sprott¹, Waldemar Kanczkowski³, Theodora Tzanavari⁶, Mohktar Bdeir¹, Sibylle Bergmann², Marc Cartellieri^{7,8}, Michael Bachmann^{7,8}, Polyxeni Nikolakopoulou³, Andreas Androutsellis-Theotokis³, Gabriele Siegert², Stefan R. Bornstein³, Michael H. Muders⁹, Louis Boon¹⁰, Katia P. Karalis^{3,6,11}, Esther Lutgens^{12,13}, Triantafyllos Chavakis^{1,2,3,4}

*equal contribution

¹⁻⁵: ¹Department of Clinical Pathobiochemistry, ²Institute for Clinical Chemistry and Laboratory Medicine, ³Department of Medicine III, ⁴Paul Langerhans Institute Dresden and ⁵Institute of Physiology; Medical Faculty, Technische Universität Dresden, Dresden, Germany; ⁶Developmental Biology Section, Biomedical Research Foundation of the Academy of Athens, Athens, Greece; ⁷Institute of Immunology, Technische Universität Dresden, Dresden, Germany; ⁸Helmholtz Zentrum Dresden-Rossendorf, Institute of Radiopharmaceutical Cancer Research, Department of Radioimmunology, Dresden, Germany; ⁹Institute of Pathology, Technische Universität Dresden, Dresden, Germany; ¹⁰Bioceros BV, Utrecht, the Netherlands; ¹¹Division of Endocrinology, Children's Hospital, Boston, MA, USA; ¹²Dept. of Medical Biochemistry, subdivision Experimental Vascular Biology, Academic Medical Center, University of Amsterdam, Amsterdam, the Netherlands; ¹³Institute for Cardiovascular Prevention (IPEK), Ludwig-Maximilians University, Munich, Germany

Email list: Antonios Chatzigeorgiou: Antonios.Chatzigeorgiou@uniklinikum-dresden.de; Kyoung-Jin Chung: Kyoung-Jin.Chung@uniklinikum-dresden.de; Ruben Garcia-Martin: Ruben.Garcia@uniklinikum-dresden.de; Ismini Alexaki: Ismini.Alexaki@uniklinikum-dresden.de; Anne Klotzsche-von Ameln: Anne.Klotzsche2@uniklinikum-dresden.de; Julia Phieler: Julia.Phieler@uniklinikum-dresden.de; David Sprott: David.Sprott@uniklinikum-dresden.de; Waldemar Kanczkowski: Waldemar.Kanczkowski@uniklinikum-dresden.de; Theodora Tzanavari: ttzanavari@bioacademy.gr; Mohktar Bdeir: mbdeir09@gmail.com; Sibylle Bergmann: Sibylle.Bergmann@uniklinikum-dresden.de; Marc Cartellieri: Marc.Cartellieri@mailbox.tu-dresden.de; Michael Bachmann: Michael.Bachmann@tu-dresden.de; Polyxeni Nikolakopoulou: Polyxeni.Nikolakopoulou@uniklinikum-dresden.de; Andreas Androutsellis-Theotokis: Andreas.Theotokis@uniklinikum-dresden.de; Gabriele Siegert: Gabriele.Siegert@uniklinikum-dresden.de; Stefan R. Bornstein: Stefan.bornstein@uniklinikum-dresden.de; Michael Muders: Michael.Muders@uniklinikum-dresden.de; Louis Boon: L.Boon@bioceros.com; Katia P. Karalis: Katia.Karalis@wyss.harvard.edu; Esther Lutgens: E.Lutgens@amc.uva.nl; Triantafyllos Chavakis: Triantafyllos.Chavakis@uniklinikum-dresden.de

Keywords: liver steatosis, adipose tissue, regulatory T cells (Tregs), inflammation

Corresponding authors

Dr. Antonios Chatzigeorgiou and Prof. Dr. Triantafyllos Chavakis
Department of Clinical Pathobiochemistry, Technische Universität Dresden,
Fetscherstrasse 74, 01307 Dresden, Germany
Email: Antonios.Chatzigeorgiou@uniklinikum-dresden.de /
Triantafyllos.Chavakis@uniklinikum-dresden.de
+49 351 458 6040

Abbreviations

Non-alcoholic steatohepatitis (NASH)
Diet-induced obesity (DIO)
Regulatory T cells (Tregs)
Adipose tissue (AT)
Non-alcoholic fatty liver disease (NAFLD)
B7.1/B7.2-double deficient mice, Double-knockout, (Dko)
Glucose tolerance test (GTT)
Insulin tolerance test (ITT)
Respiratory exchange ratio (RER)
Stromal vascular fraction (SVF)
Non-parenchymal cell (NPC)
Alanine transaminase (ALT)
Aspartate transaminase (AST)
Glutamate dehydrogenase (GLDH)

Financial Support

Supported by grants from the Deutsche Forschungsgemeinschaft (CH279/5-1 to TC and SFB 1054-B08 to EL), a European Research Council Grant (N°281296 to TC), the German Center for Diabetes Research (to TC) and the Netherlands Organization for Scientific Research (NWO)(VICI grant to EL).

Word Count (including references): 5433

ABSTRACT

The low-grade inflammatory state present in obesity contributes to obesity-related metabolic dysregulation, including non-alcoholic steatohepatitis (NASH) and insulin resistance. Intercellular interactions between immune cells or between immune cells and hepatic parenchymal cells contribute to the exacerbation of liver inflammation and steatosis in obesity. The co-stimulatory molecules B7.1 and B7.2 are important regulators of cell-cell interactions in several immune processes; however, the role of B7 co-stimulation in obesity-related liver inflammation is unknown. Here, diet-induced obesity (DIO) studies in mice with genetic inactivation of both B7.1 and B7.2 (Dko) revealed aggravated obesity-related metabolic dysregulation, reduced insulin signalling in the liver and adipose tissue (AT), glucose intolerance and enhanced progression to steatohepatitis due to B7.1/B7.2-double deficiency. The metabolic phenotype of B7.1/B7.2-double deficiency upon DIO was accompanied by increased hepatic and AT inflammation, associated with largely reduced numbers of regulatory T cells (Tregs) in these organs. In order to assess the role of B7 co-stimulation in DIO in a non-Treg lacking environment, we performed antibody-mediated inhibition of B7 molecules in wild-type mice in DIO. Antibody-blockade of both B7.1 and B7.2 improved the metabolic phenotype of DIO-mice, which was linked to amelioration of hepatic steatosis and reduced inflammation in liver and AT. *Conclusion:* Our study demonstrates a dual role of B7 co-stimulation in the course of obesity-related sequelae, particularly NASH. The genetic inactivation of B7.1/B7.2 deteriorates obesity-related liver steatosis and metabolic dysregulation likely due to the intrinsic absence of Tregs in these mice rendering Dko mice a novel murine model of NASH. In contrast, inhibition of B7 co-stimulation under conditions where Tregs are present may provide a novel therapeutic approach for obesity-related metabolic dysregulation and especially NASH.

INTRODUCTION

Obesity is associated with low-grade inflammation, liable for the development of insulin resistance, type 2 diabetes and non-alcoholic steatohepatitis (NASH). Immune cells of both the innate and adaptive immunity are implicated in this process and contribute to the development of hepatosteatosis and -steatitis as well as adipose tissue (AT) inflammation(1,2) that accompany obesity.

Inflammation in the liver is the determinant factor for the progression from non-alcoholic fatty liver disease (NAFLD), characterized by increased hepatic lipid accumulation, to NASH, featured by exacerbated intrahepatic inflammation, more intense steatosis and hepatocellular injury. Increased accumulation and activation of macrophages in the liver and activation of local Kupffer cells under obese conditions, as well as the concomitant reduction of the anti-inflammatory regulatory T cells (Tregs) are important parameters in diet-induced liver steatosis and tissue damage(3,4). Additionally, the development of AT inflammation in the course of obesity, further contributes to hepatosteatosis and deterioration of liver inflammation under obese conditions. More specifically, the accumulation of macrophages in AT and their interplay with infiltrated lymphocytes, such as cytotoxic CD8⁺ T cells, as well as the significant decrease of AT Tregs are phenomena mediating AT inflammation(1,2,5). Consecutively, cytokines/adipokines from the AT such as leptin, IL-1b or IL-18 create a crosstalk with the liver and can serve as sources of extrahepatic inflammation, thereby exacerbating hepatic steatosis(6,7). Nevertheless, the information about the exact cellular and molecular mechanisms governing obesity-related inflammation in the hepatic environment and thereby the progression of NAFLD to NASH is scarce.

CD80 and CD86 (also designated B7.1 and B7.2) are probably the best characterised co-stimulatory molecules that are mainly expressed by antigen presenting cells and interact with CD28 and CTLA-4 on T cells, mediating positive and negative signals, respectively, during T cell activation(8). The importance of B7.1 and B7.2 signalling is defined by the fact that they participate in several immunological processes such as T cell proliferation, negative selection of autoreactive T cells(9), immunoglobulin class switching(10) and Treg development(11) and are therefore implicated in several pathologies such as cancer and atherogenesis(12). The role of co-stimulation in

regulating obesity-associated inflammation has emerged from previous studies with regards to the CD40-CD40L dyad(13,14), whereas less information on the role of B7.1 and B7.2-dependent co-stimulation exists.

In this study we provide evidence that B7.1 and B7.2 have a multifaceted role in regulating obesity-related inflammatory reactions in the AT and especially in the liver and thereby the progression from NAFLD to NASH. Performing diet-induced obesity (DIO) in B7.1/B7.2-double deficient mice (Double-knockout; Dko), we observed enhanced metabolic dysregulation with glucose intolerance, insulin resistance and deterioration of hepatosteatosis associated with increased progression to hepatosteatitis, which could be ascribed to the dramatic reduction in Treg cells in B7.1/B7.2 double deficiency. Contrastingly, blocking both B7.1 and B7.2 with antibodies, but not each one alone, in wild-type mice (i.e. in the presence of normal Treg numbers) attenuated obesity-related metabolic dysregulation, improving glucose tolerance, AT inflammation and diet-induced hepatic steatosis. Together, our findings suggest a dual role of B7 co-stimulation in obesity-related steatohepatitis and metabolic dysregulation governed by the presence or absence of Tregs, and underline that B7.1-B7.2 co-stimulation may represent an interesting therapeutic target to limit obesity-related metabolic dysregulation and development of NASH.

MATERIALS AND METHODS

Detailed description of Materials and Methods is found in the Supporting Information.

RESULTS

B7.1 and B7.2 expression in obesity

To determine the presence and regulation of B7.1 and B7.2 in metabolic organs during obesity, we analyzed the mRNA expression of B7.1 and B7.2 in livers and gonadal AT from male WT mice fed a normal diet (ND) or a high-fat diet (HFD) for up to 18 weeks. Although there was no change in the expression of B7.1 or B7.2 in the total liver, we found that B7.2 was significantly upregulated in the fraction of isolated non-parenchymal cells (NPC), which largely represents the immune cell compartment of the liver (suppl.fig.1a). Moreover, both molecules were upregulated in the AT upon HFD, as well as in the stromal vascular fraction (SVF) of the AT, which contains immune cells that are resident or have infiltrated in the course of DIO

into the AT (suppl.fig.1b). These findings indicate that the expression of B7.1 and B7.2 is elevated in metabolic organs in the course of DIO, thereby implying a possible role of B7.1 and B7.2-dependent co-stimulation in the regulation of obesity-associated inflammatory processes.

B7.1-B7.2 double deficiency deteriorates obesity-related metabolic dysfunction

Considering that the co-stimulatory molecules B7.1 and B7.2 share several overlapping functional properties in regulating T-cell responses(8,10), we engaged B7 double knockout (Dko) mice, in order to study the role of B7 co-stimulation in DIO. Therefore, B7.1 and B7.2-sufficient- and –deficient (double knockout, Dko) male mice were fed a ND or a HFD. When fed a HFD, Dko mice displayed increased weight gain and food intake as compared to B7.1 and B7.2-sufficient (wild-type; WT) mice (fig.1a and suppl.Table1). Consistently, increased weight of liver and subcutaneous AT was observed in HFD-fed Dko mice (fig.1b). Although subcutaneous and gonadal AT weights were also increased in Dko mice upon ND feeding, no significant difference in body weight gain between ND-fed WT and Dko mice was observed (fig. 1a,b). In addition, metabolic cage analysis showed increased Respiratory Exchange Ratio (RER) (suppl.fig.2) in Dko mice upon HFD. These data indicate decreased lipid oxidation rates in Dko mice that could account for the increased tissue weights in these mice via higher lipid deposition. In line with these results, we found increased leptin and cholesterol levels in sera from HFD-fed Dko mice, whereas B7 double deficiency did not affect triglyceride levels (suppl.fig.3a). To clarify whether the hyperphagic phenotype of the Dko mice was linked to higher hypothalamic inflammation, we performed gene expression analysis for immune cell markers and inflammatory cytokines in hypothalami isolated from HFD-fed WT and Dko mice (suppl.fig.3b). Hypothalamic expression of inflammatory markers did not differ between WT and Dko mice (suppl.fig.3b). Thus, the hyperphagic phenotype in Dko mice is likely due to the increased levels of leptin with accelerated development of leptin resistance in these mice.

Consistently, obese Dko mice were more glucose intolerant as compared to WT mice, as assessed by a glucose tolerance test (fig.1c). In addition, an *in vivo* insulin signaling assay revealed impaired hepatic and AT insulin signaling in obese Dko mice, as indicated by decreased insulin-induced AKT-phosphorylation (suppl.fig.4).

B7.1-B7.2 double deficiency promotes diet-induced steatohepatitis

Next, we assessed the effect of B7 double-deficiency in obesity-related hepatic steatosis. Oil-Red O staining, enzymatic determination of liver triglyceride content as well as histological analysis revealed increased fat accumulation in livers from HFD-fed Dko mice, as compared to WT mice, accompanied by increased hepatocellular ballooning and histological signs of inflammation (fig.2a-e), which are key histological features of NASH. Consistently, the NAFLD activity score (NAS) was not only significantly higher in obese Dko mice as compared to WT controls (fig.2e), but also was >5, which correlates with the presence of NASH(15). That Dko mice displayed enhanced progression from hepatosteatosis to steatohepatitis was confirmed by significantly increased levels of Alanine transaminase (ALT), Aspartate transaminase (AST) and Glutamate dehydrogenase (GLDH) in the sera of HFD-fed Dko mice (fig.3a), thereby suggesting elevated liver cell injury in B7.1/B7.2 double deficiency. Similarly, HFD-fed Dko mice displayed higher levels of hepatic fibrotic injury as compared to the HFD-fed WT controls, as assessed by a Picric-acid Sirius red (Picosirius) staining analysis (fig.3b-c). Previous studies have shown that increased hepatic pro-fibrotic activity is linked to enhanced hepatic stellate cell (HSC) proliferation and mTOR activation including the activation of the p70 S6 kinase (p70S6K)(16-18). To address this point, we isolated HSC from HFD-fed WT or Dko mice and measured HSC proliferation activity by flow cytometry for PCNA and p70S6K activity by ribosomal protein S6 phosphorylation (suppl.fig.5b-c). HSC from HFD-fed Dko mice displayed increased phosphorylation of S6 ribosomal protein, suggesting enhanced activation status and pro-fibrotic activity of HSC in B7-deficiency. In contrast, no difference in PCNA staining was observed.

In concordance with these data, qPCR analysis showed significantly elevated expression of the lipogenic transcription factors SREBP1c and CHREBP and a tendency for increased expression of the lipogenic enzyme FAS and the fatty acid transporter CD36 (fig.3d) in Dko mice in DIO. Moreover, the increased expression of glucokinase and of the glucose transporter 2 (GLUT2) in the livers of Dko mice (fig.3d) in DIO is in keeping with the increased RER in B7.1/B7.2-double deficiency, as observed in the metabolic cage analysis (suppl.fig.2). Furthermore, the mRNA levels of PGC1alpha and Glut4, which are important for glucose transport in stellate

cells and thereby crucial for NASH-related fibrotic activity, were upregulated in livers from obese Dko mice (fig.3d). These data indicate greater carbohydrate utilization, enhanced lipid deposition and accelerated NASH development in the liver of Dko mice in DIO.

Given the importance of inflammation in the progression of steatosis to NASH, we analyzed hepatic inflammation in Dko and WT mice upon DIO. In addition to increased immune cell infiltration in livers of HFD-fed Dko mice, as assessed by histological evaluation (fig.2e), qPCR analysis showed increased expression of IL-1b and IL-6, although the latter did not reach significance (fig.3d).

Activated Kupffer cells, as well as Treg cells are important immune cells regulating development of NASH in an opposite fashion(4,19,20). To provide a conclusive picture about the enhanced liver inflammation in Dko mice, NPC from livers of WT and Dko mice were isolated and analyzed by flow cytometry. Dko mice displayed dramatically reduced numbers of Tregs in liver, when fed not only a HFD but also a ND (fig.4a). We also found reduced numbers of Treg cells in the blood, lymph node and spleen of Dko mice (suppl.fig.4a), but not altered numbers of CD4+ and CD8+ T cells (data not shown), as compared to WT mice, consistent with previous reports(11). This intrinsic reduction of Tregs in Dko mice explains the decreased numbers of hepatic Tregs in these mice even when fed a ND. In contrast, activated Kupffer cells (defined as F4/80+CD11b+ cells)(19), as well as dendritic cells (defined as CD11c+ cells)(21) were increased in livers from HFD-fed Dko mice, as compared to B7-sufficient mice (fig.4b,c). Concomitant with the FACS analysis data, gene expression analysis of non-parenchymal cells from WT and Dko mice showed increased expression of IL-6 and a tendency to higher levels of TNF (fig.4d). These observations suggest that higher inflammation in the livers of HFD-fed Dko mice, likely due to the reduced amounts of Tregs, contributes to increased hepatic steatosis and progression to NASH under obesity-induced conditions. Together, B7 double-deficiency deteriorates obesity-related hepatic steatosis and accelerates progression to hepatosteatitis.

Increased AT inflammation in Dko mice upon HFD

Increased AT inflammation has also been linked with obesity-related metabolic dysregulation and glucose intolerance(1,2,22). Since we found deteriorated glucose tolerance in obese Dko mice (fig.1c), we next examined AT inflammation. Flow cytometry analysis revealed decreased Treg populations in both subcutaneous and gonadal AT of HFD-fed B7-deficient mice (fig.5a). Interestingly, CD4⁺ and CD8⁺ T cells were reduced in both depots of white AT (fig.5b), implicating impaired T cell activation due to the absence of B7 co-stimulation. Despite reduced numbers of CD4⁺ and CD8⁺ T cells in the AT of Dko mice the decrease in Tregs in these mice rather prevailed to mediate a proinflammatory environment in the obese AT of these mice. In particular, increased M1 macrophages (defined as F4/80⁺CD11c⁺CD206⁻) were observed in both types of white AT in B7.1/B7.2-deficiency (fig.5d), whereas total macrophages (F4/80⁺CD11b⁺) were insignificantly higher in the AT of obese Dko mice (fig.5c). These data suggest that Dko have enhanced AT inflammation not necessarily due to increased macrophage accumulation but due to enhanced macrophage activation and polarization to the pro-inflammatory M1 phenotype, which is well in keeping with the dramatic reduction of Tregs in the AT of Dko mice. Further supporting this notion, gene expression of IL-6 was significantly increased in Dko mice, whereas the elevation of TNF and IL-12 mRNA in the gonadal AT of Dko mice almost reached significance (fig.5e). Taken together, B7.1/B7.2 double deficiency resulted in enhanced AT inflammation.

To further verify that Dko mice constitute an environment that promotes classical activation of macrophages (M1-polarization), we analyzed the inflammatory profile of thioglycollate-elicited peritoneal macrophages from WT and Dko mice by flow cytometry and qPCR. Remarkably, Dko thioglycollate-elicited macrophages had an M1-skewed phenotype, as observed by increased expression of iNOS, IL-6, reduced expression of CD206 and decreased percentage of CD206⁺ cells (suppl.fig6).

Therefore, classical activation of macrophages in Dko mice likely due to the dramatic reduction of Tregs, seems to be an additional factor for the exacerbation of obesity-related inflammation in metabolic tissues of these mice.

Adoptive transfer of Treg cells does not improve NASH and metabolic dysregulation in a B7-lacking environment

Our data so far indicated that deterioration of NASH and metabolic imbalance in Dko mice was associated with a dramatic decrease of Treg cells in these mice. A previous study has suggested that adoptive transfer of Tregs is capable of reversing obesity-related metabolic dysfunction(23). On the other hand, Tregs become highly apoptotic in a B7-lacking environment(24,25). To address whether the metabolic phenotype of Dko mice can be reversed by wild-type Tregs, Dko mice on DIO received weekly injections of isolated wild-type CD4⁺CD25⁺Tregs or control injections from the 5th week of feeding for 6 consecutive weeks. Adoptive transfer of Tregs into Dko mice failed to reverse the metabolic phenotype of Dko mice as assessed by glucose tolerance tests (suppl.fig.7). Moreover, no difference in NASH development was observed in livers from Dko mice after adoptive transfer with Tregs, as compared to control (suppl.fig.7). Liver gene expression analysis confirmed these data by showing no difference in lipogenesis- or inflammation-related genes in livers from the two groups of mice (suppl.fig.7). Consistently, flow cytometry analysis of the non-panechymal cells did not show any significant differences in hepatic and splenic Treg populations between Dko mice that received Tregs or control-treated mice (data not shown). The absence of any increase in Treg populations / numbers between Dko control-treated and Dko Treg-injected mice is in line with the fact that the B7-lacking environment is highly pro-apoptotic for Tregs(24,25), thereby explaining that wild-type Tregs fail to reverse NASH and metabolic deterioration in Dko mice.

Blocking both B7.1 and B7.2 *in vivo* improves obesity-related metabolic dysfunction

B7.1/B7.2 co-stimulatory molecules are important in activation of T cells, promoting inflammation in several conditions(8). Interestingly, our findings so far suggested that Dko mice, despite having reduced T cell activation (fig.5), rather represented a proinflammatory environment in the course of DIO, associated with reduced Treg numbers. Thereby Dko mice displayed metabolic dysregulation in DIO, including elevated glucose intolerance and enhanced progression to hepatosteatitis. We therefore hypothesized that the reduction of Tregs in Dko is responsible for skewing the system towards enhanced inflammation in DIO. However, adoptive transfer of wild-type Tregs did not reverse the development of NASH and metabolic dysregulation in Dko mice, most likely due to increased apoptosis of Treg cells in a B7-lacking environment(24,25). In order to elucidate the role of B7 co-stimulation

itself for obesity-related metabolic dysregulation in a normal, non-Treg lacking environment, we performed DIO in WT mice in the presence or absence of blocking antibodies to B7. Moreover, to determine whether B7.1 or B7.2 have distinct functions in DIO-related inflammation and metabolic changes, we treated HFD-fed WT mice either with anti-B7.1 or with anti-B7.2 or with the combination thereof. Mice were fed a HFD for a total of 16 weeks and injected with antibodies or isotype controls (twice per week) starting at week 4 of feeding. Interestingly, treatment of WT mice in DIO with anti-B7.1 or anti-B7.2 alone did not mediate any alterations in weight gain and importantly in glucose tolerance, as compared to HFD-fed isotype control-treated mice (suppl.fig.8). However, mice injected with the combination of both anti-B7.1 and anti-B7.2 antibodies displayed improved glucose tolerance and insulin sensitivity, as well as increased insulin-induced hepatic AKT-phosphorylation (suppl.fig.9), as compared to the isotype control-treated HFD-fed WT mice, although no differences in weight gain or in the weight of metabolic tissues were observed (fig.6a-c). Consistently, no difference in food intake, energy expenditure or Respiratory Exchange Ratio (RER) was observed between the two groups of mice, when metabolic cage analysis was performed (suppl.fig.10). As expected, exogenous administration of anti-B7.1 and anti-B7.2 antibodies did not affect the numbers of Tregs in mice (suppl.fig.11).

We then continued to explore whether improved glucose tolerance and insulin sensitivity due to concomitant B7.1 and B7.2 blockade in mice were also reflected by changes in AT inflammation or liver steatosis. IL-1b and IL-6 were reduced in the AT of anti-B7.1/anti-B7.2 injected mice as revealed by qPCR analysis (fig.6d). These data imply that blocking of cell-cell interactions by the antibody-mediated inhibition of B7 accounts for reduced AT inflammation. Furthermore, anti-B7.1/anti-B7.2 injected mice in DIO displayed reduced hepatic steatosis and ballooning of hepatocytes as well as reduced NAFLD activity score (fig.7a,b), while the fibro-inflammatory injury was ameliorated in these mice, as revealed by Picrosirius staining analysis (Fig.7c-d). The reduced lipid accumulation and liver damage phenotype of the anti-B7.1/anti-B7.2 injected mice was confirmed by qPCR analysis that displayed decreased levels of the fatty acid transporter CD36 and also of the steatosis-related growth factor TGF-beta(26) (fig.8a). As in lymphoid organs and the AT (suppl.fig.11 and data not shown), Treg cell population in the liver was also not affected by

B7.1/B7.2 blockade, as assessed by *foxp3* gene expression (fig.8a). Interestingly, inflammatory markers such as IL-6 and IL-1 β were significantly decreased in mice injected with anti-B7.1/anti-B7.2 (fig.8a).

Decreased inflammatory activation by B7.1/B7.2 blockade could be due to inhibition of the communication of hepatocytes and/or antigen-presenting cells with T cells within the liver micro-environment. To verify this hypothesis, we simulated the liver environment under obese conditions *in vitro* and performed hepatocyte-NPC co-cultures in the presence of palmitate, while cell-cell interactions were blocked with the combination of anti-B7.1 and anti-B7.2. Reduced IL-6, IL-1 β and TNF were detected in supernatants of co-cultures when anti-B7.1 and anti-B7.2 were applied, as compared to the isotype control treated co-cultures (fig.8b). These data imply that B7 co-stimulation could mediate intercellular communication between hepatocytes and immune cells, thereby potentially triggering hepatic inflammation in DIO.

Taken together, concomitant blockade of B7.1 and B7.2 in the presence of Tregs improves glucose tolerance, insulin sensitivity, hepatic steatosis as well as AT and liver inflammation, thus suggesting B7 co-stimulation itself contributes to obesity-related inflammation and metabolic dysregulation.

DISCUSSION

Co-stimulatory molecules play a major role in the intercellular communication of adaptive immune cells with antigen-presenting cells, innate immune cells or parenchymal cells(8,27,28). A plethora of cell-cell interactions take place in liver and AT in the course of obesity, regulating inflammation and thereby the development of steatohepatitis and insulin resistance(1,2,20,29,30). Here, we identified B7-dependent co-stimulation as a major regulator of obesity-related inflammatory processes and metabolic dysregulation(1,2). B7.1/B7.2 double-deficiency exacerbated the development of NASH and metabolic dysregulation upon DIO, a phenotype attributed to the absence of Treg cells in liver and AT of these mice. In contrast, antibody-mediated blockade of B7 interactions under conditions, where regulatory T cells are present, protected mice from the development of obesity-related pathologies and especially NASH.

In the course of obesity, Dko mice displayed a deteriorated metabolic phenotype. Importantly, Dko mice displayed increased hepatic steatosis, hepatocellular ballooning, deteriorated hepatic insulin signalling and enhanced progression to hepatosteatitis/NASH. Inflammation constitutes the second hit in the prevailing 2-hit theory for the pathogenesis of NASH, in which lipid accumulation is followed by a second stimulus that triggers the evolution of steatosis to steatitis(4,19,20). Activated Kupffer cells in the liver mediate obesity-related liver inflammation, mainly by producing cytokines such as TNF, IL-6 and IL-1b(20,29,31). Likewise, the reduction of Tregs and/or of the anti-inflammatory cytokine IL-10 in the liver promotes liver inflammation(4,32). The pro-inflammatory hepatic features associated with NASH development were exacerbated in B7-double deficiency. The dramatic decrease in Treg numbers in the blood and lymphoid tissues of Dko mice due to the absolute requirement of B7 co-stimulation for Treg survival and proliferation(11,33) resulted in the absence of Tregs from metabolic organs (liver, AT). The B7-deficient environment is “toxic“ to Tregs, as was evidenced by the failure of adoptive transfer of wild-type Tregs to reverse the metabolic phenotype of Dko mice, as compared to wild-type mice in DIO(23). Consistent with increased Treg apoptosis in B7-negative environment(24,25), no increase in Treg numbers was found in the lymphoid and metabolic organs of B7-deficient mice upon adoptive Treg transfer. Together, due to the absence of Tregs, deficiency of B7 co-stimulation promoted a pro-inflammatory environment in the liver with increased numbers of activated Kupffer cells and enhanced proinflammatory gene expression. Our findings are in line with those of Ma et al. that demonstrated a connection between Treg reduction and the development of liver steatosis under obese conditions(4). Together, the early and exacerbated NASH development in B7.1/B7.2 double deficiency also indicates that Dko may represent a feasible mouse model for studying NASH in future studies.

Consistently, HFD-fed Dko mice displayed higher levels of hepatic fibro-inflammatory injury. Isolated HSC from Dko mice displayed increased phosphorylation of S6 ribosomal protein, suggesting enhanced pro-fibrotic activity(16-18), whereas we did not find significantly elevated HSC proliferation due to B7-deficiency. The latter could be due to the fact that only one time point (15 weeks on HFD) was used for proliferation analysis of isolated HSC. A detailed time kinetic analysis comparing stellate cell proliferation and activation in WT and Dko

mice on a HFD and ND for different time points would be necessary to fully address this issue in a future study.

Accumulating evidence underlines the role of leptin in NASH development mainly via immune cell activation in NAFLD(34,35). The increased levels of leptin accompanied by reduced Treg numbers in B7 Dko mice are in line with the already established reciprocal relationship between leptin levels and Treg proliferation(36-38). Thus, in our study, the enhanced leptin levels in B7 Dko mice likely contributed to the progression to steatohepatitis in these mice.

In addition to hepatosteatitis, metabolic parameters such as glucose tolerance or insulin signalling were worse in B7-deficient mice. Metabolic deterioration in B7-deficient mice was associated with significantly higher AT inflammation, as assessed by the enhanced M1 polarization of macrophages in the AT and increased expression of pro-inflammatory cytokines, such as TNF and IL-6 that act to mediate AT insulin resistance(2,31). Interestingly, the AT environment in Dko mice was pro-inflammatory despite reduced accumulation of effector T cells (CD4+ and CD8+ cells), as B7 co-stimulation is an important effector for T cell activation. Together, our data suggest that, although co-stimulation is indispensable for T cell activation, the diminution of Tregs in metabolic organs of Dko is hierarchically the driving force triggering liver and AT inflammation in DIO, thereby leading to hepatosteatitis and glucose intolerance.

To further support the notion that the dramatic reduction in Tregs accounted for aggravation of steatohepatitis and metabolic deterioration in Dko mice and could over-ride any beneficial effects of disruption of B7-dependent co-stimulation, we blocked B7 interactions under conditions where Tregs were present. To this end, we exogenously administered anti-B7.1 and anti-B7.2 antibodies into wild-type mice in DIO. The use of B7 blockade was the only possible experimental approach to address Treg-independent functions of B7 co-stimulation in DIO, given our finding that adoptive transfer of wild-type Treg cells was not operative in the B7-negative environment, although this approach has been previously engaged to ameliorate obesity-related AT inflammation and metabolic dysregulation in B7-sufficient wild-type settings(23,39). The improvement of metabolic dysregulation and reduced

hepatosteatosis/hepatosteatitis by concomitant antibody-mediated inhibition of both B7.1 and B7.2 in DIO but not by inhibiting each one alone suggests a synergistic action of B7.1 and B7.2 to promote obesity-related inflammation. B7 co-stimulation was found to mediate interactions between hepatocytes and NPC, which are important for the initiation and progress of inflammation in the intrahepatic environment(40). In particular, anti-B7.1/B7.2 blockade reduced the expression of inflammatory cytokines in hepatocyte-NPC co-cultures. Moreover, blocking B7 interactions alleviated AT inflammation, in keeping with recent studies that identified adipocytes as antigen-presenting cells(41). A previous study has manipulated the B7/CD28/CTLA-4 co-stimulation by using CTLA-4-Ig; this treatment did not significantly improve steatohepatitis or metabolic dysregulation in DIO(42). While our manuscript was in preparation, a study appeared showing that B7-double deficiency is linked to enhanced AT inflammation and insulin resistance; in contrast, this study did not report the hepatic phenotype of B7-double deficiency(43). Based on their findings with Dko mice, these authors concluded that B7 co-stimulation protects from insulin resistance. However, our approach to block B7.1 and B7.2 in the presence of Tregs in WT mice uncovered that B7-costimulation in fact promotes obesity-related metabolic dysregulation and NASH. We therefore conclude that intercellular B7 co-stimulatory interactions contribute to the exacerbation of inflammation in liver and AT during DIO. However, in Dko mice the absence of Tregs simply masked any beneficial anti-inflammatory effects that could derive from inactivation of B7 co-stimulation.

In conclusion, the present study identified that B7.1 and B7.2 co-stimulation plays important roles in obesity-related inflammation, glucose intolerance and hepatosteatitis. Genetic inactivation and antibody inhibition of CD80/CD86 co-stimulatory molecules affect obesity-related hepatosteatitis and metabolic dysregulation in an opposite fashion, which is orchestrated by the numbers and function of Tregs. Our findings not only underline the importance of Tregs as a master regulator of obesity-driven liver inflammation, but also indicate that inhibition of B7 co-stimulation may provide a novel platform for potential therapeutic manipulation for the prevention of NASH and likely other obesity-related complications.

ACKNOWLEDGEMENTS

The authors would like to thank Maria Moissidou, Sylvia Grossklaus, Janine Gebler, Bettina Gercken, Marta Prucnal and Christine Mund for technical assistance.

References

1. Chatzigeorgiou A, Karalis KP, Bornstein SR, Chavakis T. Lymphocytes in obesity-related adipose tissue inflammation. *Diabetologia* 2012;55:2583-2592.
2. Chmelar J, Chung KJ, Chavakis T. The role of innate immune cells in obese adipose tissue inflammation and development of insulin resistance. *Thromb Haemost* 2013;109:399-406.
3. Cusi K. Role of obesity and lipotoxicity in the development of nonalcoholic steatohepatitis: pathophysiology and clinical implications. *Gastroenterology* 2012;142:711-725 e716.
4. Ma X, Hua J, Mohamood AR, Hamad AR, Ravi R, Li Z. A high-fat diet and regulatory T cells influence susceptibility to endotoxin-induced liver injury. *Hepatology* 2007;46:1519-1529.
5. Winer S, Chan Y, Paltser G, Truong D, Tsui H, Bahrami J, Dorfman R, et al. Normalization of obesity-associated insulin resistance through immunotherapy. *Nat Med* 2009;15:921-929.
6. Duval C, Thissen U, Keshtkar S, Accart B, Stienstra R, Boekschoten MV, Roskams T, et al. Adipose tissue dysfunction signals progression of hepatic steatosis towards nonalcoholic steatohepatitis in C57BL/6 mice. *Diabetes* 2010;59:3181-3191.
7. Schaffler A, Scholmerich J, Buchler C. Mechanisms of disease: adipocytokines and visceral adipose tissue--emerging role in nonalcoholic fatty liver disease. *Nat Clin Pract Gastroenterol Hepatol* 2005;2:273-280.
8. Ceeraz S, Nowak EC, Noelle RJ. B7 family checkpoint regulators in immune regulation and disease. *Trends Immunol* 2013.
9. Buhlmann JE, Elkin SK, Sharpe AH. A role for the B7-1/B7-2:CD28/CTLA-4 pathway during negative selection. *J Immunol* 2003;170:5421-5428.
10. Borriello F, Sethna MP, Boyd SD, Schweitzer AN, Tivol EA, Jacoby D, Strom TB, et al. B7-1 and B7-2 have overlapping, critical roles in immunoglobulin class switching and germinal center formation. *Immunity* 1997;6:303-313.
11. Zeng M, Guinet E, Nouri-Shirazi M. B7-1 and B7-2 differentially control peripheral homeostasis of CD4(+)CD25(+)Foxp3(+) regulatory T cells. *Transpl Immunol* 2009;20:171-179.
12. Buono C, Pang H, Uchida Y, Libby P, Sharpe AH, Lichtman AH. B7-1/B7-2 costimulation regulates plaque antigen-specific T-cell responses and atherogenesis in low-density lipoprotein receptor-deficient mice. *Circulation* 2004;109:2009-2015.
13. Chatzigeorgiou A, Seijkens T, Zarzycka B, Engel D, Poggi M, van den Berg S, van den Berg S, et al. Blocking CD40-TRAF6 signaling is a therapeutic target in obesity-associated insulin resistance. *Proc Natl Acad Sci U S A* 2014;111:2686-2691.
14. Poggi M, Engel D, Christ A, Beckers L, Wijnands E, Boon L, Driessen A, et al. CD40L deficiency ameliorates adipose tissue inflammation and metabolic manifestations of obesity in mice. *Arterioscler Thromb Vasc Biol* 2011;31:2251-2260.
15. Kleiner DE, Brunt EM, Van Natta M, Behling C, Contos MJ, Cummings OW, Ferrell LD, et al. Design and validation of a histological scoring system for nonalcoholic fatty liver disease. *Hepatology* 2005;41:1313-1321.

16. Caligiuri A, Bertolani C, Guerra CT, Aleffi S, Galastri S, Trappoliere M, Vizzutti F, et al. Adenosine monophosphate-activated protein kinase modulates the activated phenotype of hepatic stellate cells. *Hepatology* 2008;47:668-676.
17. Xu WH, Hu HG, Tian Y, Wang SZ, Li J, Li JZ, Deng X, et al. Bioactive compound reveals a novel function for ribosomal protein S5 in hepatic stellate cell activation and hepatic fibrosis. *Hepatology* 2014.
18. Wang Y, Gao J, Zhang D, Zhang J, Ma J, Jiang H. New insights into the antifibrotic effects of sorafenib on hepatic stellate cells and liver fibrosis. *J Hepatol* 2010;53:132-144.
19. Tosello-Tramont AC, Landes SG, Nguyen V, Novobrantseva TI, Hahn YS. Kupffer cells trigger nonalcoholic steatohepatitis development in diet-induced mouse model through tumor necrosis factor-alpha production. *J Biol Chem* 2012;287:40161-40172.
20. Stienstra R, Saudale F, Duval C, Keshtkar S, Groener JE, van Rooijen N, Staels B, et al. Kupffer cells promote hepatic steatosis via interleukin-1beta-dependent suppression of peroxisome proliferator-activated receptor alpha activity. *Hepatology* 2010;51:511-522.
21. Connolly MK, Bedrosian AS, Mallen-St Clair J, Mitchell AP, Ibrahim J, Stroud A, Pachter HL, et al. In liver fibrosis, dendritic cells govern hepatic inflammation in mice via TNF-alpha. *J Clin Invest* 2009;119:3213-3225.
22. Lumeng CN, Bodzin JL, Saltiel AR. Obesity induces a phenotypic switch in adipose tissue macrophage polarization. *J Clin Invest* 2007;117:175-184.
23. Eller K, Kirsch A, Wolf AM, Sopper S, Tagwerker A, Stanzl U, Wolf D, et al. Potential role of regulatory T cells in reversing obesity-linked insulin resistance and diabetic nephropathy. *Diabetes* 2011;60:2954-2962.
24. Bar-On L, Birnberg T, Kim KW, Jung S. Dendritic cell-restricted CD80/86 deficiency results in peripheral regulatory T-cell reduction but is not associated with lymphocyte hyperactivation. *Eur J Immunol* 2011;41:291-298.
25. Zou T, Caton AJ, Koretzky GA, Kambayashi T. Dendritic cells induce regulatory T cell proliferation through antigen-dependent and -independent interactions. *J Immunol* 2010;185:2790-2799.
26. Yadav H, Quijano C, Kamaraju AK, Gavrilova O, Malek R, Chen W, Zervas P, et al. Protection from obesity and diabetes by blockade of TGF-beta/Smad3 signaling. *Cell Metab* 2011;14:67-79.
27. Chen L. Co-inhibitory molecules of the B7-CD28 family in the control of T-cell immunity. *Nat Rev Immunol* 2004;4:336-347.
28. Chatzigeorgiou A, Lyberi M, Chatzilymperis G, Nezos A, Kamper E. CD40/CD40L signaling and its implication in health and disease. *Biofactors* 2009;35:474-483.
29. De Taeye BM, Novitskaya T, McGuinness OP, Gleaves L, Medda M, Covington JW, Vaughan DE. Macrophage TNF-alpha contributes to insulin resistance and hepatic steatosis in diet-induced obesity. *Am J Physiol Endocrinol Metab* 2007;293:E713-725.
30. Tang Y, Bian Z, Zhao L, Liu Y, Liang S, Wang Q, Han X, et al. Interleukin-17 exacerbates hepatic steatosis and inflammation in non-alcoholic fatty liver disease. *Clin Exp Immunol* 2011;166:281-290.
31. Chawla A, Nguyen KD, Goh YP. Macrophage-mediated inflammation in metabolic disease. *Nat Rev Immunol* 2011;11:738-749.

32. Feuerer M, Herrero L, Cipolletta D, Naaz A, Wong J, Nayer A, Lee J, et al. Lean, but not obese, fat is enriched for a unique population of regulatory T cells that affect metabolic parameters. *Nat Med* 2009;15:930-939.
33. Bour-Jordan H, Bluestone JA. Regulating the regulators: costimulatory signals control the homeostasis and function of regulatory T cells. *Immunol Rev* 2009;229:41-66.
34. Chatterjee S, Ganini D, Tokar EJ, Kumar A, Das S, Corbett J, Kadiiska MB, et al. Leptin is key to peroxynitrite-mediated oxidative stress and Kupffer cell activation in experimental non-alcoholic steatohepatitis. *J Hepatol* 2013;58:778-784.
35. Procaccini C, Galgani M, De Rosa V, Carbone F, La Rocca C, Ranucci G, Iorio R, et al. Leptin: the prototypic adipocytokine and its role in NAFLD. *Curr Pharm Des* 2010;16:1902-1912.
36. De Rosa V, Procaccini C, Cali G, Pirozzi G, Fontana S, Zappacosta S, La Cava A, et al. A key role of leptin in the control of regulatory T cell proliferation. *Immunity* 2007;26:241-255.
37. Procaccini C, De Rosa V, Galgani M, Abanni L, Cali G, Porcellini A, Carbone F, et al. An oscillatory switch in mTOR kinase activity sets regulatory T cell responsiveness. *Immunity* 2010;33:929-941.
38. Matarese G, Procaccini C, De Rosa V, Horvath TL, La Cava A. Regulatory T cells in obesity: the leptin connection. *Trends Mol Med* 2010;16:247-256.
39. Deiluiis J, Shah Z, Shah N, Needleman B, Mikami D, Narula V, Perry K, et al. Visceral adipose inflammation in obesity is associated with critical alterations in regulatory cell numbers. *PLoS One* 2011;6:e16376.
40. Scott MJ, Liu S, Su GL, Vodovotz Y, Billiar TR. Hepatocytes enhance effects of lipopolysaccharide on liver nonparenchymal cells through close cell interactions. *Shock* 2005;23:453-458.
41. Hruskova Z, Biswas SK. A new "immunological" role for adipocytes in obesity. *Cell Metab* 2013;17:315-317.
42. Montes VN, Turner MS, Subramanian S, Ding Y, Hayden-Ledbetter M, Slater S, Goodspeed L, et al. T cell activation inhibitors reduce CD8+ T cell and pro-inflammatory macrophage accumulation in adipose tissue of obese mice. *PLoS One* 2013;8:e67709.
43. Zhong J, Rao X, Braunstein Z, Taylor A, Narula V, Hazey J, Mikami D, et al. T-cell costimulation protects obesity-induced adipose inflammation and insulin resistance. *Diabetes* 2013;63:1289-1302.

Legends to figures**Figure 1****Metabolic profile of B7.1-B7.2 Dko mice**

Wild type (WT) and Dko male mice were fed with normal-fat (ND) or high-fat diet (HFD). A) Body weight gain of WT and Dko mice on ND or HFD in grams. B) Subcutaneous AT, gonadal AT and liver weights of WT and Dko mice after 18 weeks on ND or HFD are displayed as percentage of total body weight. C) Glucose tolerance test in WT and Dko mice fed a ND or HFD for 17 weeks was performed as described under Materials and Methods. Data are mean±SEM; n=10-19; *p<0.05 (comparisons between WT and Dko mice fed the same diet).

Figure 2**Increased hepatosteatitis in Dko mice upon HFD**

A) Oil red O staining in liver cryosections from WT and Dko mice fed a ND or HFD for 18 weeks is shown (A) (x100 magnification). B) The Oil-Red O positive area was evaluated by using the ImageJ software and expressed as percentage of the total area (n=at least 4). Data are mean±SEM, *p<0.05 for comparison between WT and Dko mice fed the same diet. C) Liver triglyceride content was quantified in WT and Dko mice fed a ND or HFD for 18 weeks (n=at least 5 for ND and n=at least 14 for HFD). Data are mean±SEM, *p<0.05 for comparison between WT and Dko mice fed the same diet. D) Representative H&E staining in liver paraffin sections from WT and Dko mice fed a HFD for 18 weeks is shown (x100 magnification). E) Histological scoring of NASH in liver sections from WT and Dko mice fed a HFD for 18 weeks was done as described under Materials and Methods. Steatosis and inflammation were scored using a 0 to 3 scale while ballooning by using a 0 to 2 scale according to the NASH-CRN Committee scoring system (n=at least 6). The NAFLD activity score (NAS) is defined as the sum of steatosis, lobular inflammation and ballooning. Data are mean±SEM, *p<0.05.

Figure 3**Increased liver damage in Dko mice upon HFD**

A) Serum alanine transaminase (ALT), aspartate transaminase (AST) and glutamate dehydrogenase (GLDH) activities in sera from WT and Dko mice fed a HFD for 18 weeks (n=at least 10). B) Representative Picrosirius staining in liver sections from

WT and Dko mice fed a HFD for 18 weeks (x100 magnification). C) The Picrosirius positive area was evaluated by using the ImageJ software and expressed as percentage of the total area (n=6). D) Liver gene expression analysis from WT or Dko mice fed a HFD for 18 weeks. Shown are mRNA levels of genes related to lipogenesis (SREBP1C, Sterol Regulatory Element-Binding Protein; CHREBP, Carbohydrate-responsive element-binding protein; FAS, fatty acid synthase), lipid uptake (CD36), glucose uptake and metabolism (GLUT2, Glucose transporter 2; GCK, glucokinase, GLUT4, Glucose transporter 4; PPAR- γ , Peroxisome proliferator-activated receptor gamma; PGC1a, PPAR- γ coactivator 1-alpha) and inflammation (IL-6, IL-1b). The mRNA expression was normalized against 18S and the gene expression of livers from WT mice under HFD was set as 1 (n=6). Data are mean \pm SEM, *p<0.05.

Figure 4

Increased hepatic inflammation in Dko mice upon HFD

A-C) WT or Dko male mice were fed a ND or HFD for 14 weeks and non-parenchymal cells (NPC) were isolated from livers and analyzed by flow cytometry. A) Treg cells (defined as CD4+CD25+Foxp3+); B) Kupffer cells (defined as CD11b+F4/80+); and C) dendritic cells (defined as CD11c+) are shown. Cells were expressed as absolute cell number per liver. Treg cells were additionally expressed as percentage of CD4 positive cells (n= 5). Data are mean \pm SEM, *p<0.05, for comparison between WT and Dko mice fed the same diet. D) qPCR analysis for TNF, IL-6 and MCP-1 in NPC isolated from WT or Dko male mice fed a HFD for 14 weeks (n= 5 mice). The mRNA expression was normalized against actin and the gene expression of non-parenchymal cells from WT HFD was set as 1. Data are mean \pm SEM, *p<0.05.

Figure 5

B7 double deficiency aggravates AT inflammation

SVF (stromal vascular fraction) cells from subcutaneous (sub) or gonadal (gon) AT of WT or Dko male mice fed a HFD for 18 weeks were isolated and analyzed by flow cytometry. A-D) Treg cells (defined as CD4+CD25+Foxp3+) (A), CD3+CD4+ or CD3+CD8+ lymphocytes (B), macrophages (characterized as CD11b+F4/80+) (C) and M1-macrophages (defined as F4/80+CD11c+CD206-) (D) were detected. Cells were expressed as cells per gram of tissue. Treg cells were additionally expressed as

percentage of CD4 positive cells (n=at least 7). Data are mean±SEM, *p<0.05. E) Gonadal AT gene expression analysis from WT or Dko mice fed a ND or HFD for 18 weeks. The mRNA levels of TNF, IL-6, IL-12 and MCP-1 are shown. 18S was used for normalization of mRNA expression and the gene expression of WT ND was set as 1. n= 5/group for ND and n= 7/group for HFD. Data are mean±SEM, *p<0.05 for comparison between WT and Dko mice fed the same diet.

Figure 6

Blocking B7.1 and B7.2 with antibodies in vivo improved obesity-related metabolic dysregulation

WT male mice were fed a HFD for a total of 16 wks and received a combination of anti-B7.1 and anti-B7.2 antibodies (anti-B7.1/B7.2 WT mice) or isotype controls (CTRL WT mice) starting at week 4 of feeding (200µg of each antibody or isotype control were injected intraperitoneally per mouse, twice per week). A) Body weight of HFD-fed mice treated with antibodies or isotype controls is displayed in grams. B) Glucose and insulin tolerance tests were performed in weeks 15 and 16 of feeding, respectively, as described under Materials and Methods. C) Subcutaneous and gonadal AT and liver weight of WT mice treated with anti-B7.1/B7.2 or isotype control antibodies are displayed in grams. Data are mean±SEM; (n= at least 8); *p<0.05. D) Gene expression analysis of inflammatory genes and leptin was performed in gonadal AT from the two groups of mice. The mRNA expression was normalized against 18S and the gene expression of isotype control-injected mice was set as 1 (n=at least 6). Data are mean ± SEM, *p<0.05.

Figure 7

Anti-B7.1 and B7.2 treatment improves obesity-related liver damage

WT male mice were fed a HFD for a total of 16 wks, receiving a combination of anti-B7.1 and anti-B7.2 antibodies (anti-B7.1/B7.2 WT mice) or isotype controls (CTRL WT mice) starting at week 4 of feeding (200µg of each antibody or isotype control were injected intraperitoneally per mouse, twice per week). A) Representative H&E staining in liver paraffin sections from CTRL WT and anti-B7.1/B7.2 WT mice (x100 magnification). B) Histological scoring of NASH in liver sections from CTRL WT and anti-B7.1/B7.2 WT mice was done as described under Materials and Methods. Steatosis and inflammation were scored using a 0 to 3 scale, while ballooning by

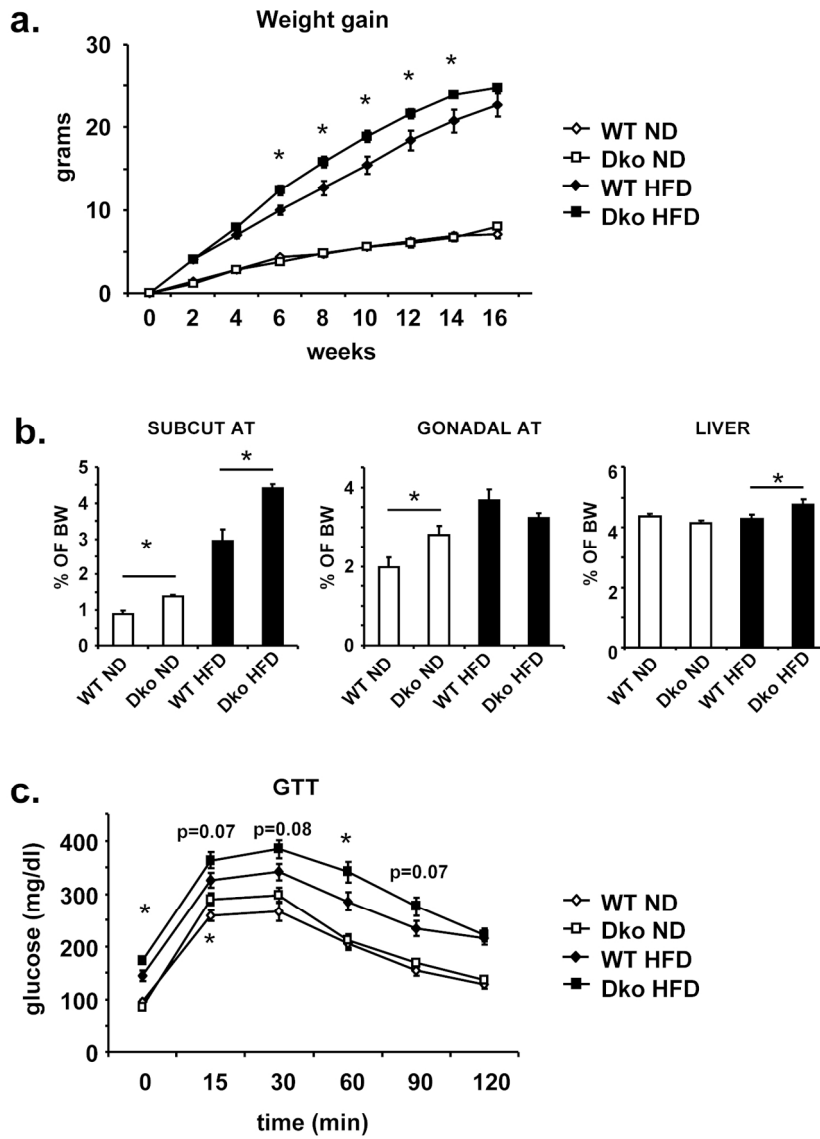
using a 0 to 2 scale. The NAFLD activity score (NAS) represents the sum of steatosis, lobular inflammation and ballooning. n= 6. C) Representative Picrosirius staining in liver sections from CTRL WT and anti-B7.1/B7.2 WT mice is shown (x100 magnification). D) The Picrosirius positive area was evaluated by using the ImageJ software and expressed as percentage of the total area (n=6). Data are mean±SEM, *p<0.05.

Figure 8

Anti-B7.1 and B7.2 treatment improved liver inflammation

A) WT male mice were fed a HFD for a total of 16 wks and received from week 4 of the feeding a combination of anti-B7.1 and anti-B7.2 antibodies or isotype controls (200µg of each antibody or isotype control were injected intraperitoneally per mouse, twice per week). The mRNA levels of lipid accumulation-related genes (CD36, TGF- β), inflammatory genes (IL-6, TNF, IL-1 β) and of the transcription factor FOXP3 were analyzed by qPCR. 18S expression was used for normalization of mRNA expression and the gene expression of CTRL-WT mice was set as 1 (n= at least 7). Data are mean±SEM, *p<0.05. B) Hepatocytes and Non-Parenchymal Cells (NPC) were isolated from livers of WT mice and co-cultured for 24 hours with 500µmol/l palmitate and in the presence of a combination of anti-B7.1/B7.2 antibodies or isotype controls as described under Materials and Methods. The levels of secreted cytokines were detected in supernatants by ELISA (n= at least 5). Data are mean±SEM, *p<0.05.

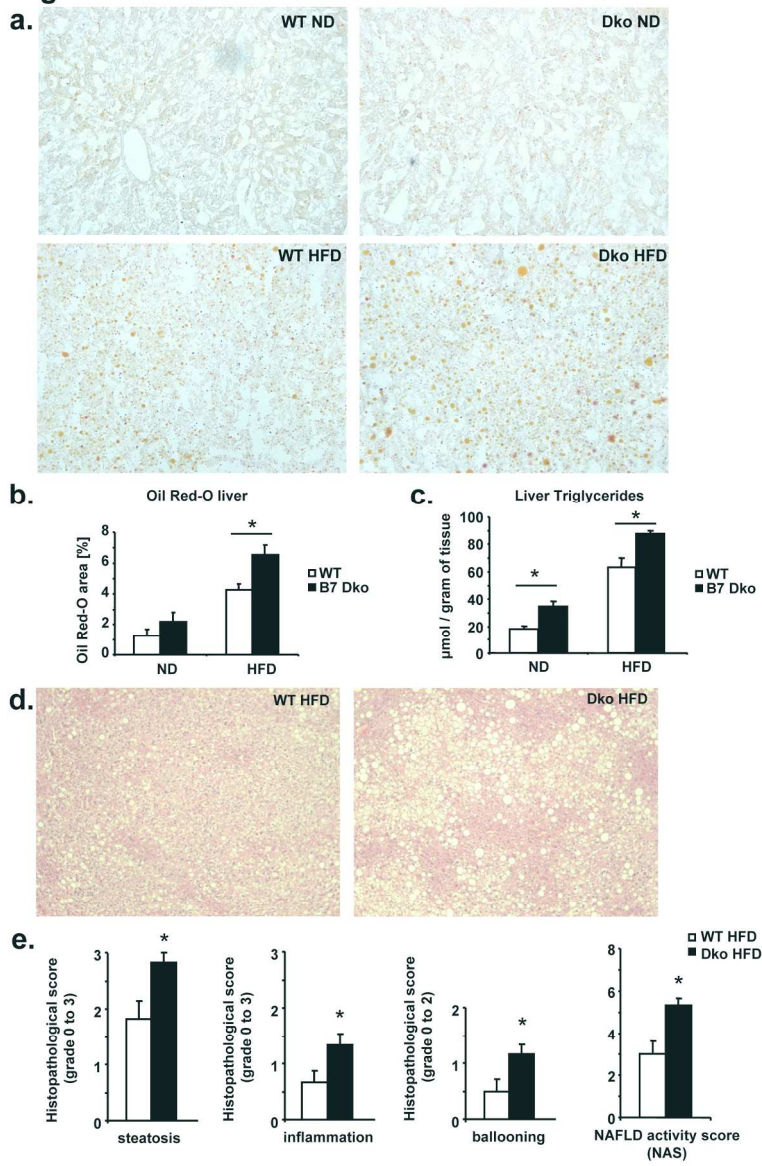
Figure 1



126x180mm (300 x 300 DPI)

AC

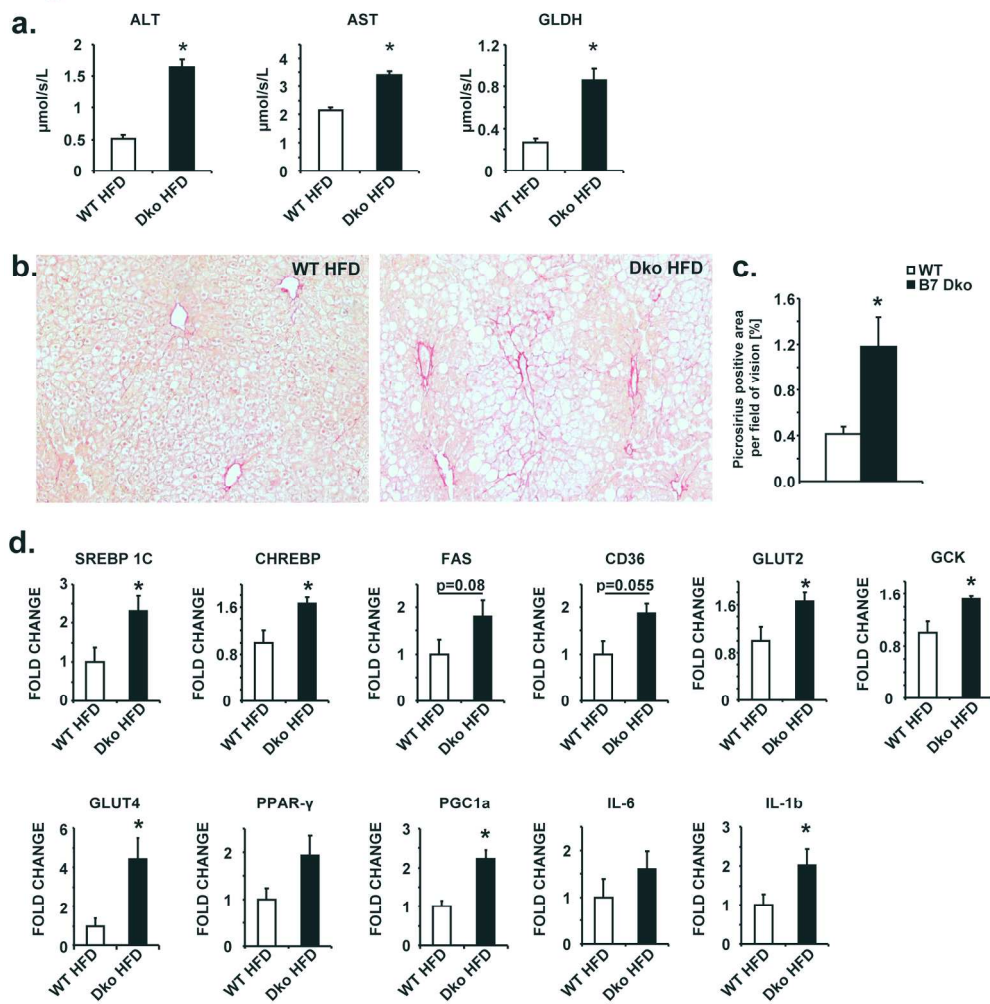
Figure 2



150x233mm (300 x 300 DPI)

AC

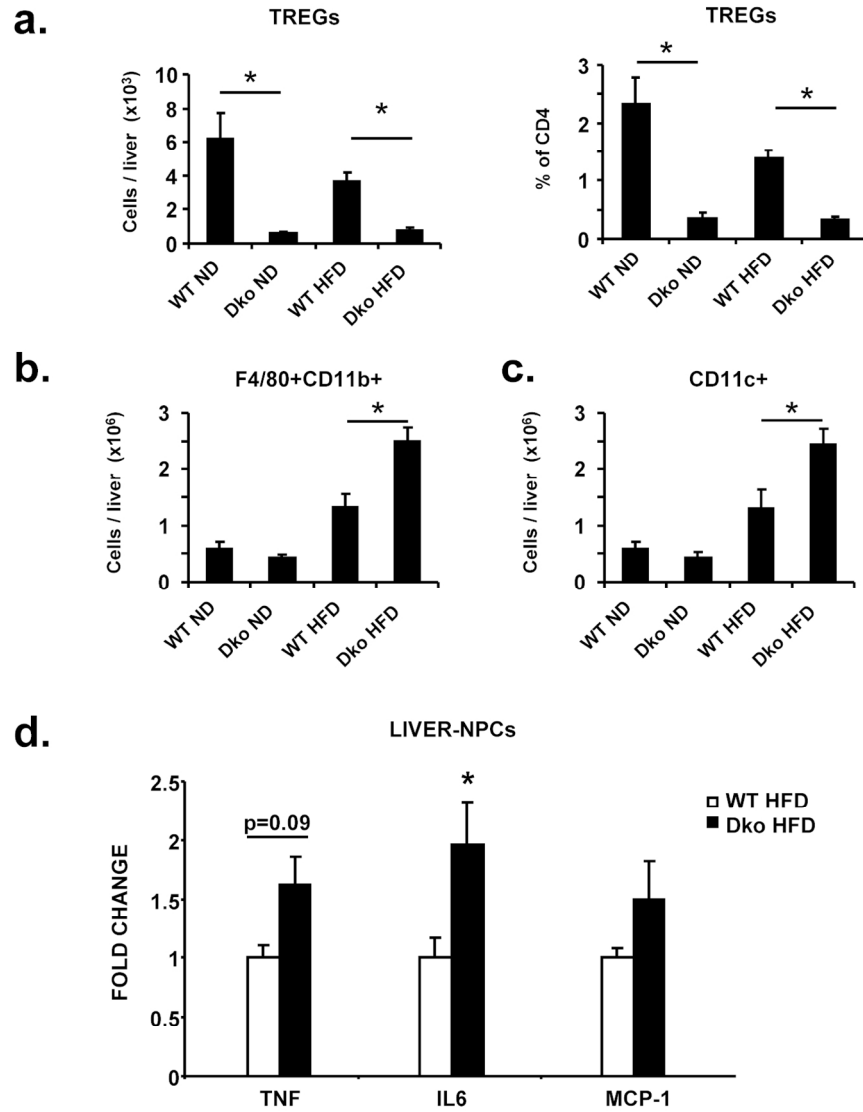
Figure 3



180x189mm (300 x 300 DPI)

Acc

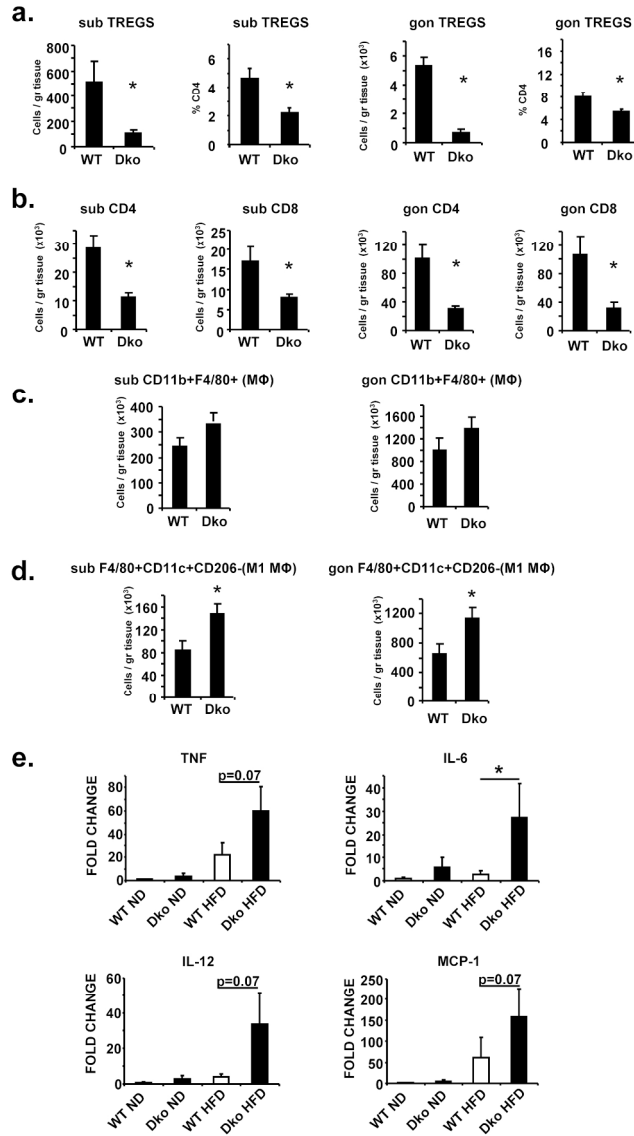
Figure 4



118x157mm (300 x 300 DPI)

AC

Figure 5



133x244mm (300 x 300 DPI)

AC

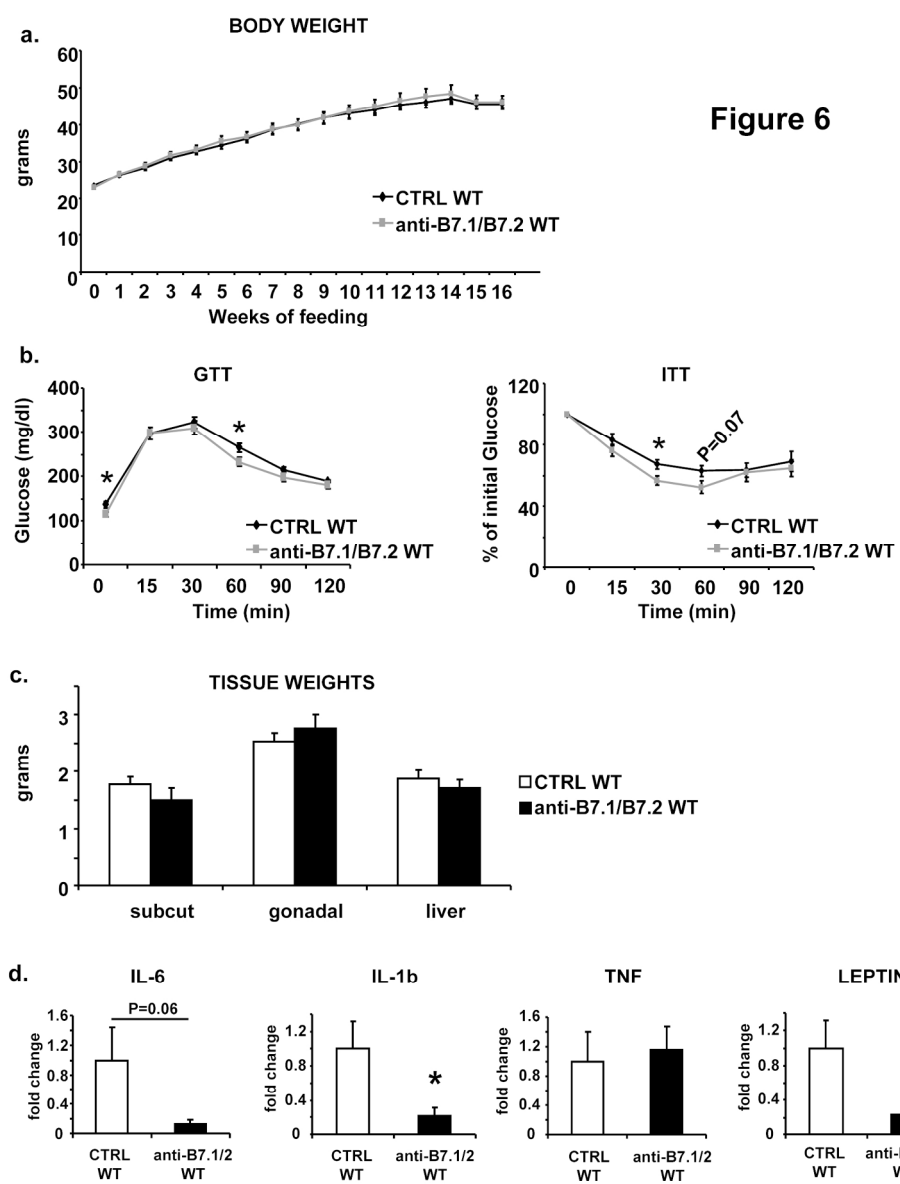
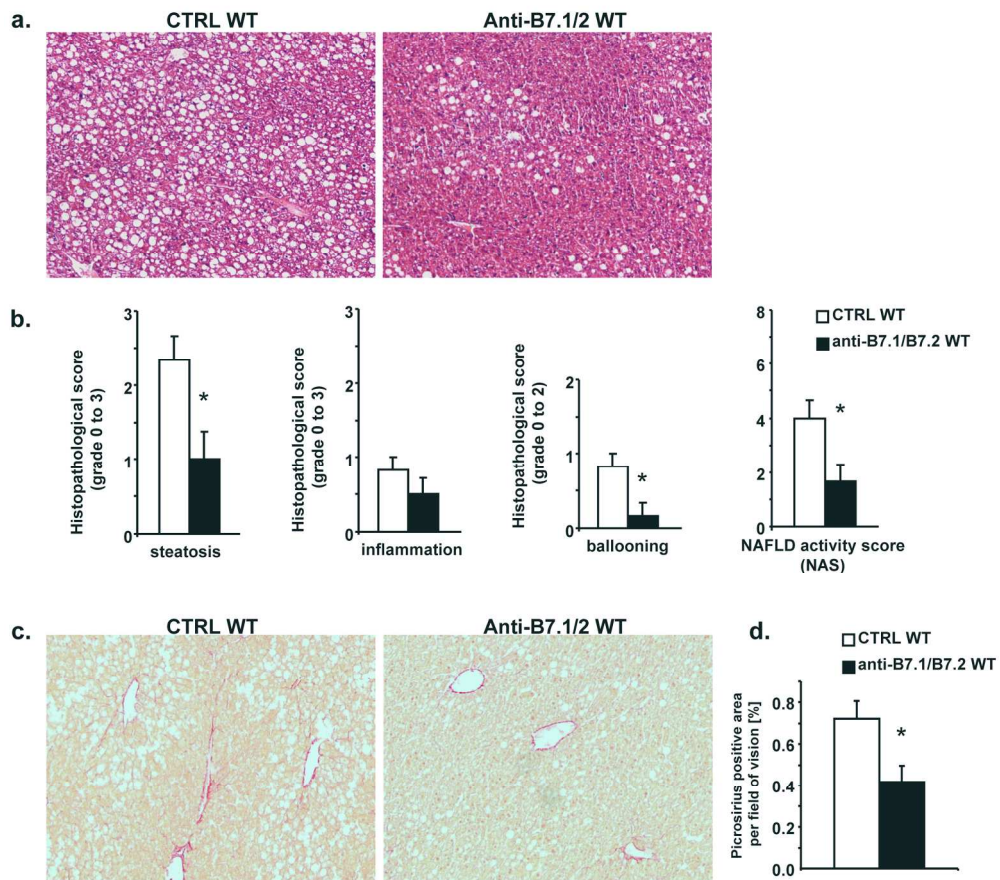


Figure 6

174x217mm (300 x 300 DPI)

AC

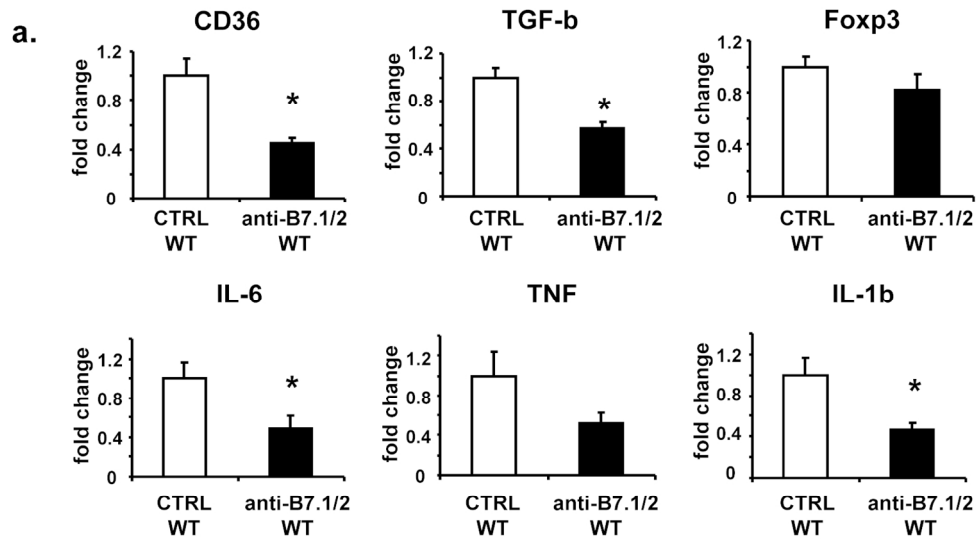
Figure 7



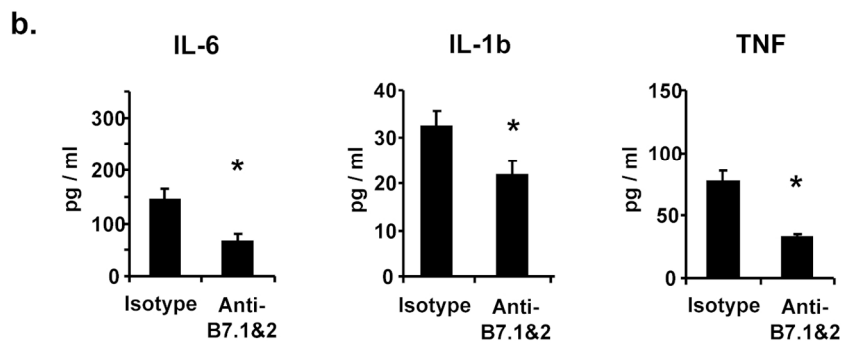
173x166mm (300 x 300 DPI)

Acce

Figure 8



Hepatocytes – NPC coculture



135x145mm (300 x 300 DPI)

ACC

Supporting Information

Dual role of B7 costimulation in obesity-related non-alcoholic steatohepatitis (NASH) and metabolic dysregulation

Antonios Chatzigeorgiou^{1,2,3,4,*}, Kyoung-Jin Chung^{1,5,*}, Ruben Garcia-Martin¹, Ismini Alexaki¹, Anne Klotzsche-von Ameln^{1,5}, Julia Phieler^{1,4}, David Sprott¹, Waldemar Kanczkowski³, Theodora Tzanavari⁶, Mohktar Bdeir¹, Sibylle Bergmann², Marc Cartellieri^{7,8}, Michael Bachmann^{7,8}, Polyxeni Nikolakopoulou³, Andreas Androutsellis-Theotokis³, Gabriele Siegert², Stefan R. Bornstein³, Michael H. Muders⁹, Louis Boon¹⁰, Katia P. Karalis^{3,6,11}, Esther Lutgens^{12,13}, Triantafyllos Chavakis^{1,2,3,4}

*equal contribution

^{1-5:} ¹Department of Clinical Pathobiochemistry, ²Institute for Clinical Chemistry and Laboratory Medicine, ³Department of Medicine III, ⁴Paul Langerhans Institute Dresden and ⁵Institute of Physiology; Medical Faculty, Technische Universität Dresden, Dresden, Germany; ⁶Developmental Biology Section, Biomedical Research Foundation of the Academy of Athens, Athens, Greece; ⁷Institute of Immunology, Technische Universität Dresden, Dresden, Germany; ⁸Helmholtz Zentrum Dresden-Rossendorf, Institute of Radiopharmaceutical Cancer Research, Department of Radioimmunology, Dresden, Germany; ⁹Institute of Pathology, Technische Universität Dresden, Dresden, Germany; ¹⁰Bioceros BV, Utrecht, the Netherlands; ¹¹Division of Endocrinology, Children's Hospital, Boston, MA, USA; ¹²Dept. of Medical Biochemistry, subdivision Experimental Vascular Biology, Academic Medical Center, University of Amsterdam, Amsterdam, the Netherlands; ¹³Institute for Cardiovascular Prevention (IPEK), Ludwig-Maximilians University, Munich, Germany

MATERIALS AND METHODS

Animal studies and diets

Mice deficient in both B7.1 and B7.2 (double knockouts, Dko) in a C57BL/6 background, kindly provided by Dr. R. Hodes (Experimental Immunology Branch, NCI, NIH), were previously described (1, 2). C57BL/6 mice were used as wild-type controls (WT). WT and Dko mice were bred and co-housed in our facility for several generations. Male mice sufficient or deficient in B7.1 and B7.2 were fed a normal-fat diet or high-fat diet (D12450B, 10% fat or D12492, 60% fat respectively, Research Diets, NJ, USA) for up to 18 weeks starting at the age of 7-8 weeks. In other experiments, regulatory T cells were adoptively transferred into Dko mice that were fed a high-fat diet for a total of 12 weeks. The intraperitoneal injections of Tregs (or PBS as control) into Dko mice were performed once per week for 6 consecutive weeks, starting at week 5 of the HFD feeding; 0.75×10^6 Tregs were transferred per injection per mouse. Treg isolation for this purpose is described below under "Treg isolation from spleen".

Additionally, C57BL/6 mice were fed a HFD for 16 weeks and injected either with anti-B7.1 alone or with anti-B7.2 alone or with a combination of anti-B7.1 and anti-B7.2 antibodies or isotypes (twice per week, 200 μ g/mouse of each antibody or isotype, Bioceros, Utrecht, Netherlands) starting at week 4 of HFD feeding. After the experimental period, mice were euthanized and tissues and blood were collected and either processed immediately or stored in -80°C for further analysis. All animal experiments were performed according to the criteria outlined in the "Guide for the Care and Use of Laboratory Animals", published by the National Institutes of Health (NIH). All animal experiments were approved by the Landesdirektion Dresden, Germany.

Metabolic tests

Blood glucose, triglycerides and cholesterol were measured in overnight fasted mice by tail-vein blood sampling and by using a glucose meter device (Accu-Chek, Roche, Mannheim, Germany) and the Accutrend Plus system (Roche, Mannheim, Germany), respectively. For glucose tolerance test (GTT), overnight-fasted mice were injected i.p. with glucose (1g/kg). For insulin tolerance test (ITT), 5-6 h fasted mice were injected

i.p. with insulin (1.5U/kg, Huminsulin, Lilly, Bad Homburg, Germany). Glucose levels were measured in both tests at 0, 15, 30, 60, 90 and 120 minutes post injection.

Metabolic cage analysis

Mice were individually housed in metabolic cages (PhenoMaster, TSE Systems, Bad Homburg, Germany) with free access to water and food, maintaining a 12h:12h light-dark cycle. A period of at least 24 hours acclimatization in the metabolic cages preceded initiation of the experiment and data collection. Volume of oxygen consumption (VO_2) and carbon dioxide production (VCO_2) were determined every 20 minutes. Respiratory exchange ratio (RER) was calculated as VCO_2/VO_2 , whereas energy expenditure (EE) was determined using the formula $3.941 \times VO_2 + 1.106 \times VCO_2$ (3). Locomotion as well as food and water intakes were also monitored. Data were normalized with respect to body weight using ANCOVA analysis.

Serum and supernatant parameters

Mouse serum or culture supernatant parameters were measured by using commercially available kits. More specifically, leptin, IL-6, IL-1b and TNF were measured with kits from R&D. Alanine transaminase (ALT), Aspartate transaminase (AST) and Glutamate dehydrogenase (GLDH) were measured in sera in a Roche Modular P800 Analyzer.

Measurement of liver triglyceride content

Triglyceride quantification in the liver was done by using a commercially available kit (Abcam, Cambridge, UK). Briefly, 100mg of tissue was homogenized in 1ml of 5% Triton-X100 in water and the samples were then heated to 95°C and cooled to room temperature twice. After centrifugation, triglyceride determination in the supernatants was done enzymatically.

***In vivo* insulin-induced phospho-AKT activation analysis**

The *in vivo* phospho-AKT signaling study was performed as described previously (4). Briefly, WT and DKO mice or isotype- and anti-B7.1/B7.2 treated mice fed with HFD were fasted overnight prior to an intraperitoneal injection of 2 U/kg insulin (Lilly). After 7 minutes, liver and gonadal adipose tissues were collected and snap frozen in

liquid nitrogen. Cell lysates were prepared and western blot analysis was performed by using antibodies against phospho-AKT (phospho-AKT–Ser473, Cell Signaling, Germany) and total AKT (Cell Signaling, Germany). The band intensity was quantified by using the ImageJ software and the insulin-induced phospho-AKT was evaluated by normalization over total AKT signaling.

Hepatocyte and non-parenchymal cell (NPC) isolation

Isolation of hepatocytes and non-parenchymal cells (NPC) was done according to previously published protocols with some modifications (5-7). After systemic perfusion of mice, livers were excised, minced and incubated in DMEM containing crude collagenase and hyaluronidase (Sigma Aldrich, Munich, Germany) at 37°C for 30min. The suspension was passed through a 100 µm strainer and hepatocytes were separated from NPC by centrifuging at 50g for 3min. NPC were washed with DMEM, treated with RBC lysis buffer (5min, RT) and washed again 3x at 200g for 10min to remove debris. Both hepatocytes and NPC were used for further procedures.

Hepatic stellate cells isolation and proliferation activity assay

Primary mouse hepatic stellate cells (HSC) were isolated as described previously (8). Briefly, WT and DKO mice fed a HFD for 15 weeks were anesthetized and perfusion of the liver through the portal vein was performed by using consecutively EGTA, Pronase E (0.5mg/ml, Sigma Aldrich) and Collagenase P (0.4mg/ml, Roche Diagnostics, Germany) containing buffers. The separated livers were further digested by a Pronase E (1mg/ml), collagenase P (0.4mg/ml) and DnaseI (2mg/ml, Roche Diagnostics, Germany) containing solution and filtered through a 70µm cell strainer. After washing with Gey's balanced salt solution including DnaseI, HSC were purified from other hepatic cells and debris by centrifugation on a 8% Nycodenz gradient (Progen Biotechnik, Germany) at 1500g, for 15min, at 4°C without break. After washing, the separated HSC were stained with an anti-mouse CD45-PE antibody (eBioscience), fixed and permeabilized and further stained against proliferating cell nuclear antigen (PCNA)-FITC (Milipore) and phospho-S6 Ribosomal protein (Ser235/236)-Alexa Fluor 647 (Cell signaling). The CD45 negative and PCNA positive or pS6 positive cells were detected by flow cytometry on a FACS Canto II (BD, Heidelberg, Germany).

Adipose-tissue (AT) stromal vascular fraction (SVF) isolation

Stromal vascular fraction (SVF) isolation was performed as previously described (4). Briefly, subcutaneous or gonadal AT from euthanized mice were isolated, minced and incubated at 37°C in DMEM containing collagenase type I (2 mg/ml per gram of tissue; Invitrogen, Darmstadt, Germany). The suspension was resuspended in DMEM-0.5% BSA (Sigma Aldrich, Munich, Germany), centrifuged so as to separate adipocytes from the SVF, incubated then for 5 min with RBC lysis buffer (eBioscience, Frankfurt, Germany), and washed again before further analysis.

Flow cytometry analysis

For flow cytometry analysis, cells were resuspended in FACS buffer (HBSS Solution with 0.1% BSA and 0.1% NaN₃) and filtered through a 40 µm cell strainer. Fc-blocking (CD16/32 antibody, BD, Heidelberg, Germany) was applied and cells were stained with antibodies against CD4, CD8, CD3, CD25, FoxP3, CD11b, CD11c, F4/80, and CD206 purchased from Miltenyi Biotec (Bergisch Gladbach, Germany), eBiosciences (San Diego, CA, USA) BioLegend (Fell, Germany) or Acris Antibodies (Herford, Germany). Overnight fixation of cells with a fixation / permeabilization buffer (eBioscience, Frankfurt, Germany) was used when staining for CD206 or Foxp3 was performed. Flow cytometry was performed on a FACS Canto II (BD, Heidelberg, Germany) and data were analyzed by using FACSDiva Version 6.1.3 software.

Treg isolation from spleen

Splenic cells were isolated from 8 week old mice and stained with anti-CD3e-PE, anti-CD4-FITC and anti-CD25-APC (Miltenyi Biotec). After pooling, the CD4⁺CD25⁺-Treg cells were sorted using a FACS Aria II cell sorter (BD Biosciences). The sorted cells were collected into PBS with 0.5% BSA, washed twice with PBS and then injected into Dko mice (0.75x10⁶ cells/mouse/week) as described under “Animal Studies and diets”. The purity of Treg cells was routinely >90%.

Peritoneal macrophage polarization analysis

Macrophage polarization was studied in peritoneal macrophages. Briefly, peritonitis was induced in 8 week old male wild type or Dko mice by intraperitoneal injection of 1ml 3% thioglycollate (9, 10). After 3 days, macrophages were isolated by peritoneal

lavage with 15 ml 3% FBS PBS per mouse. Isolated cells were analyzed by FACS analysis for F4/80, CD11b and CD206 and by real-time PCR.

Co-culture experiments

For hepatocyte-liver NPC co-culture, cells were isolated as described above under “Hepatocyte and non-parenchymal cell (NPC) isolation”. Hepatocytes were plated overnight into 12-well collagen coated culture plates (3×10^5 cells / well), while NPC were incubated in suspension culture dishes in complete-DMEM containing 300 ng/ml LPS. On day 2, both cell populations were washed with DMEM and NPC (10^6 cells / well) were added into plates containing hepatocytes. The cells were co-cultured for 24h in palmitate (500 μ mol/l)-containing medium in the absence or presence of a combination of anti-B7.1 and anti-B7.2 or respective isotype controls (Bioceros, Utrecht, Netherlands) and supernatants were collected for further analysis. Palmitate preparation was done as described previously (11).

Real-Time PCR analysis

Total RNA was extracted with Trizol (Invitrogen, Darmstadt, Germany) and cDNA was synthesized with the iScript cDNA Synthesis Kit (Bio-Rad, Munich, Germany). PCRs were performed with a Bio-Rad cycler system (BioRad, Munich, Germany) using the SsoFast EvaGreen Supermix (BioRad) and gene-specific primers. The relative amount of the different mRNAs were quantified with the $\Delta\Delta$ Ct method while the expression of 18S or actin mRNA was used for normalization among samples (12). The fold-change ratio was calculated.

Immunohistochemistry and immunofluorescence

For conventional light microscopy, livers were fixed in 4% paraformaldehyde solution overnight at 4°C. Tissues were embedded in paraffin, cut into 5 μ m thick sections and subjected to hematoxylin / eosin and Picric acid Sirius red (Picosirius) staining. The level of NAFLD/NASH was read blinded to experimental design and the degree of steatosis, lobular inflammation, ballooning was evaluated according to previously published criteria following the NASH-CRN Committee scoring system (13). Steatosis and inflammation were scored using a 0 to 3 scale, while ballooning by using a 0 to 2 scale. The NAFLD activity score (NAS) was defined as the sum of steatosis, lobular inflammation and ballooning, thus ranging from 0 to 8.

For histochemical staining with Oil Red O (ORO), 10 µm cryosections were prepared, slides were fixed in ice-cold 10% formalin solution for 10 minutes, rinsed in dH₂O and stained for 15 minutes in ORO in 60% isopropanol solution (ORO:H₂O, 3:2). Slides were then rinsed in 60% isopropanol and nuclei were counter-stained with Mayer's haematoxylin. Slides were rinsed in H₂O and mounted with 95% glycerol.

A microscope coupled to a computerized system (Zeiss, Oberkochen, Germany) and equipped with the AxioVision Rel. 4.8 software (Carl-Zeiss MicroImaging GmbH, Jena, Germany) was used for the aforementioned experimental procedures. The Oil-Red O or Picrosirius red positive areas were evaluated by using the ImageJ software (14).

Statistical analysis

Data are expressed as means ± SEM and a Student's T-Test or a Mann-Whitney *U* test were used. The GTT and ITT results were analyzed by a 2-way ANOVA.

Significance was set at $P < 0.05$.

References

1. Borriello F, Sethna MP, Boyd SD, Schweitzer AN, Tivol EA, Jacoby D, Strom TB, et al. B7-1 and B7-2 have overlapping, critical roles in immunoglobulin class switching and germinal center formation. *Immunity* 1997;6:303-313.
2. Vacchio MS, Williams JA, Hodes RJ. A novel role for CD28 in thymic selection: elimination of CD28/B7 interactions increases positive selection. *Eur J Immunol* 2005;35:418-427.
3. Arch JR, Hislop D, Wang SJ, Speakman JR. Some mathematical and technical issues in the measurement and interpretation of open-circuit indirect calorimetry in small animals. *Int J Obes (Lond)* 2006;30:1322-1331.
4. Phieler J, Chung KJ, Chatzigeorgiou A, Klotzsche-von Ameln A, Garcia-Martin R, Sprott D, Moissidou M, et al. The complement anaphylatoxin c5a receptor contributes to obese adipose tissue inflammation and insulin resistance. *J Immunol* 2013;191:4367-4374.
5. Scott MJ, Liu S, Su GL, Vodovotz Y, Billiar TR. Hepatocytes enhance effects of lipopolysaccharide on liver nonparenchymal cells through close cell interactions. *Shock* 2005;23:453-458.
6. Tang Y, Bian Z, Zhao L, Liu Y, Liang S, Wang Q, Han X, et al. Interleukin-17 exacerbates hepatic steatosis and inflammation in non-alcoholic fatty liver disease. *Clin Exp Immunol* 2011;166:281-290.
7. Stienstra R, Saudale F, Duval C, Keshtkar S, Groener JE, van Rooijen N, Staels B, et al. Kupffer cells promote hepatic steatosis via interleukin-1beta-dependent

- suppression of peroxisome proliferator-activated receptor alpha activity. *Hepatology* 2010;51:511-522.
8. Maschmeyer P, Flach M, Winau F. Seven steps to stellate cells. *J Vis Exp* 2011;10.
 9. Choi EY, Orlova VV, Fagerholm SC, Nurmi SM, Zhang L, Ballantyne CM, Gahmberg CG, et al. Regulation of LFA-1-dependent inflammatory cell recruitment by Cbl-b and 14-3-3 proteins. *Blood* 2008;111:3607-3614.
 10. Chavakis T, Athanasopoulos A, Rhee JS, Orlova V, Schmidt-Woll T, Bierhaus A, May AE, et al. Angiostatin is a novel anti-inflammatory factor by inhibiting leukocyte recruitment. *Blood* 2005;105:1036-1043.
 11. Chatzigeorgiou A, Phielers J, Gebler J, Bornstein SR, Chavakis T. CD40L Stimulates the Crosstalk Between Adipocytes and Inflammatory Cells. *Horm Metab Res* 2013;45:741-747.
 12. Livak KJ, Schmittgen TD. Analysis of relative gene expression data using real-time quantitative PCR and the 2⁻(Delta Delta C(T)) Method. *Methods* 2001;25:402-408.
 13. Kleiner DE, Brunt EM, Van Natta M, Behling C, Contos MJ, Cummings OW, Ferrell LD, et al. Design and validation of a histological scoring system for nonalcoholic fatty liver disease. *Hepatology* 2005;41:1313-1321.
 14. Rasband WS. ImageJ, U. S. National Institutes of Health, Bethesda, Maryland, USA, <http://imagej.nih.gov/ij/>, . 1997-2012.

Legends to supplementary figures

Suppl. Figure 1

Regulation of B7.1-B7.2 expression in obesity

A) B7.1 and B7.2 gene expression was analyzed in liver and hepatic non-parenchymal cells (NPC) of WT male mice fed a ND or HFD for 15 weeks. The mRNA expression was normalized against 18S and the gene expression in liver or NPC from ND-fed mice was set as 1 (n= 5). Data are mean ± SEM, *p<0.05. B) B7.1 and B7.2 gene expression analysis was performed by qPCR in gonadal AT and stromal vascular fraction (SVF) from gonadal AT of WT male mice fed a normal (ND) or high fat (HFD) diet for 18 weeks. The mRNA expression was normalized to 18S and the B7.1/B7.2 expression under ND conditions served as control and was set as 1 (n= 5). Data are mean ± SEM, *p<0.05.

Suppl. Figure 2

Metabolic cage analysis in WT and Dko mice

WT or Dko mice fed a ND or HFD for 8 weeks were housed in metabolic cages maintaining a 12h:12h light-dark cycle with free access to water and food. After

acclimatization (24 hours), volume of oxygen consumption (VO_2) and carbon dioxide production (VCO_2), respiratory exchange ratio (RER), energy expenditure (EE), locomotion and food and water intakes were monitored. Black bars mean dark cycles whereas white bars represent light cycles. $n=3$ /group for ND and $n=5$ /group for HFD. Data are mean \pm SEM, $*p<0.05$ for comparison between WT and Dko mice fed the same diet.

Suppl. Figure 3

A) Metabolic parameters of WT and Dko mice fed a HFD for 18 weeks. WT and Dko male mice were fed a HFD for a total of 18 weeks. The levels of leptin were measured by ELISA in sera (after sacrificing mice), while blood cholesterol and triglycerides were quantified by tail-vein blood sampling, 1-2 weeks before sacrificing the mice as described under Materials and Methods (n =at least 12). Data are mean \pm SEM, $*p<0.05$.

B) Hypothalamic inflammation in WT and Dko mice fed a HFD.

Hypothalami from WT and Dko fed a HFD for 8 weeks were isolated and the mRNA expression of cellular and inflammatory markers were analyzed by qPCR. The mRNA expression was normalized against 18S and the gene expression of wild type mice was set as 1 ($n=4$). Data are mean \pm SEM.

Suppl. Figure 4

Insulin signaling in liver and white AT of WT and Dko mice

WT and Dko male mice were fed a HFD for 17 weeks. Mice were fasted overnight, insulin (2U/Kg) was injected intraperitoneally and tissues were collected after 7 min for immunoblotting. (A, C) Representative western blot analysis of insulin-induced AKT phosphorylation as well as total AKT from liver (A) and gonadal AT (C) is shown. (B, D) Densitometric analysis of the phosphorylated AKT/total AKT ratio in liver (B) and gonadal AT (D) is shown. Data are mean \pm SEM, $*p<0.05$ for comparison between WT and Dko mice ($n=4$).

Suppl. Figure 5

A. B7.1-B7.2 Dko mice have reduced numbers of Treg cells

Total leukocytes were isolated from lymph node, spleen and blood of male WT and B7-double deficient (Dko) mice and analyzed by flow cytometry.

CD4⁺CD25⁺Foxp3⁺ Treg cells are depicted as percentage of total leukocytes from lymph node, spleen and blood (n=4). Data are mean \pm SEM, *p<0.05.

B,C. Increased hepatic stellate cell activity in Dko mice

Hepatic stellate cells (HSC) were isolated from livers of WT and Dko mice fed a HFD for 15 weeks. The freshly isolated HSC were analyzed by flow cytometry and CD45⁻ cells were analysed for PCNA (B) or pS6 (C). Percentages of PCNA⁺ or pS6⁺ among the isolated stellate cell population as well as the mean fluorescence intensities (MFI) of PCNA or pS6 are shown. Data are mean \pm SEM, *p<0.05 (n=5/group). PCNA: proliferating cell nuclear antigen, pS6: phospho-S6 ribosomal protein.

Suppl. Figure 6

Macrophage polarization in WT vs Dko mice

Thioglycollate-elicited peritoneal macrophages were isolated from 8 week old male WT or Dko mice. A,B) Cells isolated by peritoneal lavage were stained for CD11b, F4/80 and CD206. CD206 was analyzed in CD11b⁺F4/80⁺ cells. A) Percentage of CD206⁺ cells and mean fluorescence values from WT and Dko mice. B) The gene expression of iNOS and IL-6 (M1-macrophages markers) in isolated cells from peritoneal lavage from WT and Dko mice was analysed by qPCR. The mRNA expression was normalized against 18S and the relative gene expression (gene expression / 18S expression ratio) is depicted (n= at least 6). Data are mean \pm SEM, *p<0.05.

Suppl. Figure 7

Adoptive transfer of Treg cells does not reverse hepatic steatosis or metabolic dysregulation due to B7-deficiency

Dko male mice were fed a HFD for 12 weeks, receiving 6 intraperitoneal injections of 0.75×10^6 FACS-sorted CD4⁺CD25⁺ Treg cells (once per week starting from week 5 until week 10) or control injections with PBS. A) Body weight of PBS- or Treg-injected Dko mice (Dko-CTRL and Dko-Treg-INJ mice, respectively) in grams is depicted. B) Glucose tolerance test after 11 weeks of feeding as described under Materials and Methods. C) Representative H&E staining in liver paraffin sections from PBS- or Treg-injected Dko mice is shown (x100 magnification). D) The mRNA

levels of lipid accumulation related genes (SREBP1C, Sterol Regulatory Element-Binding Protein; CHREBP, Carbohydrate-responsive element-binding protein; TGF- β , Transforming growth factor-beta) and inflammatory genes (TNF, IL-1 β) were analyzed by qPCR. 18S expression was used for normalization of mRNA expression and the gene expression of PBS-injected mice (Dko CTRL) was set as 1. Data are mean \pm SEM; n= 5.

Suppl. Figure 8

Antibody blockade of either B7.1 or B7.2 does not affect obesity-related metabolic dysregulation

WT male mice were fed a HFD for a total of 16 weeks, receiving either anti-B7.1 or anti-B7.2 antibodies or respective isotype controls starting at week 4 of feeding (200 μ g of each antibody or isotype control were injected intraperitoneally per mouse, twice per week). (A) Body weight of HFD-fed anti-B7.1 or isotype control-injected mice in grams is depicted (n=at least 8) B) glucose and insulin tolerance tests of HFD-fed anti-B7.1 or isotype control-injected mice were performed in weeks 15 and 16 of feeding, respectively, as described under Materials and Methods (n=at least 8). C) Body weight of HFD-fed anti-B7.2 or isotype control-injected mice in grams is depicted (n=at least 6). D) Glucose and insulin tolerance tests of HFD-fed anti-B7.2 or isotype control-injected mice were performed in weeks 15 and 16 of feeding, respectively, as described under Materials and Methods (n=at least 6). Data are mean \pm SEM.

Suppl. Figure 9

Antibody-mediated B7 blockade improved hepatic insulin signaling.

WT male mice were fed a HFD for a total of 11 weeks and received a combination of anti-B7.1 and anti-B7.2 antibodies (anti-B7.1/B7.2 WT mice) or isotype controls (CTRL WT mice) starting at week 4 of feeding (200 μ g of each antibody or isotype control were injected intraperitoneally per mouse, twice per week).

Mice were fasted overnight, insulin (2U/Kg) was injected intraperitoneally and tissues were collected after 7 min for immunoblotting. (A) Representative western blot analysis of insulin-induced AKT phosphorylation as well as total AKT from liver is

shown. (B) Densitometric analysis of the phosphorylated AKT/total AKT ratio is shown. Data are mean \pm SEM (n=4).

Suppl. Figure 10. Metabolic cage analysis in isotype- and anti-B7.1/B7.2 treated mice

WT male mice were fed a HFD for 8 weeks and also received a combination of anti-B7.1 and anti-B7.2 antibodies (anti-B7.1/B7.2 WT mice) or isotype controls (CTRL WT mice) starting at week 4 of feeding (200 μ g of each antibody or isotype control were injected intraperitoneally per mouse, twice per week). Mice were then transferred to metabolic cages. After acclimatization (24h), respiratory exchange ratio (RER) (A), energy expenditure (EE) (B), food intake (C) and locomotion (D) were assessed in a metabolic monitoring system maintaining a 12h:12h light-dark cycle with free access to water and food for 3 days. Data are mean \pm SEM; n= 3.

Suppl. Figure 11

Splenic Treg population does not change in HFD-fed mice upon anti-B7.1 and anti-B7.2 treatment

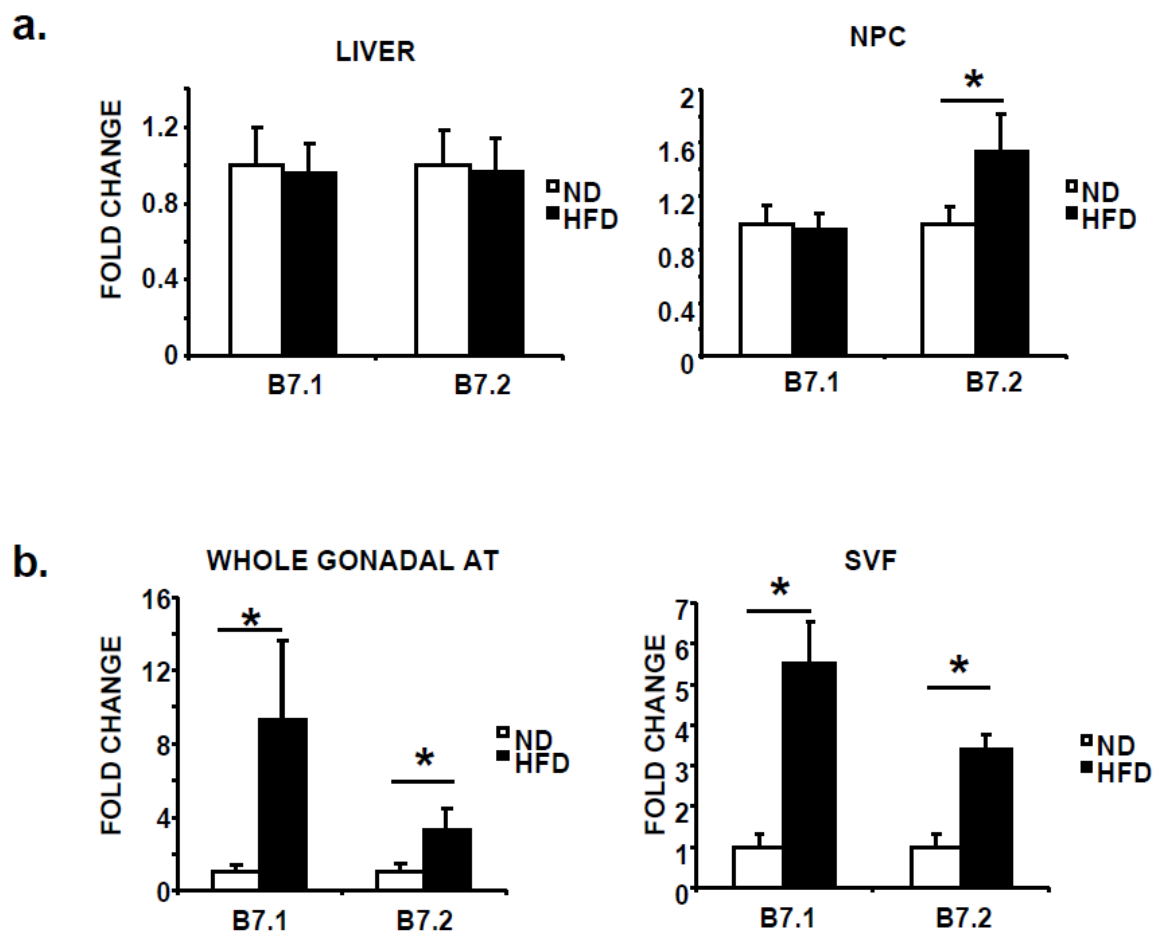
WT male mice were fed a HFD for a total of 16 weeks and also received a combination of anti-B7.1 and anti-B7.2 antibodies (anti-B7.1/B7.2 WT mice) or isotype controls (CTRL WT mice) starting at week 4 of feeding (200 μ g of each antibody or isotype control were injected intraperitoneally per mouse, twice per week). Total leukocytes from spleen were isolated and CD4+CD25+Foxp3+ Treg cells were detected by FACS. Tregs are expressed as percentage of the total leukocytes isolated from spleen (n=8). Data are mean \pm SEM.

Suppl. Table 1**Metabolic cage analysis in WT and Dko mice under normal or high-fat diet**

	ND		HFD	
	WT	DKO	WT	DKO
VO2 light (mL/h)	100.8 ± 3.8	104.2 ± 1.1	116.6 ± 2.8	127.3 ± 6.3
VO2 dark (mL/h)	120.8 ± 1.2	121.9 ± 1.7	134.5 ± 7.0	141.6 ± 8.7
VCO2 light (mL/h)	91.1 ± 5.6	97.8 ± 4.2	85.2 ± 1.9	94.9 ± 5.0
VCO2 dark (mL/h)	116.1 ± 0.6	120.7 ± 1.3	99.8 ± 4.6	107.8 ± 7.3
Food intake (g/h)	0.112 ± 0.007	0.121 ± 0.007	0.023 ± 0.006	0.039 ± 0.009 *
Water intake (mL/h)	0.100 ± 0.006	0.142 ± 0.015	0.075 ± 0.010	0.067 ± 0.009

Values represent Mean ± SEM. * p-value < 0.05

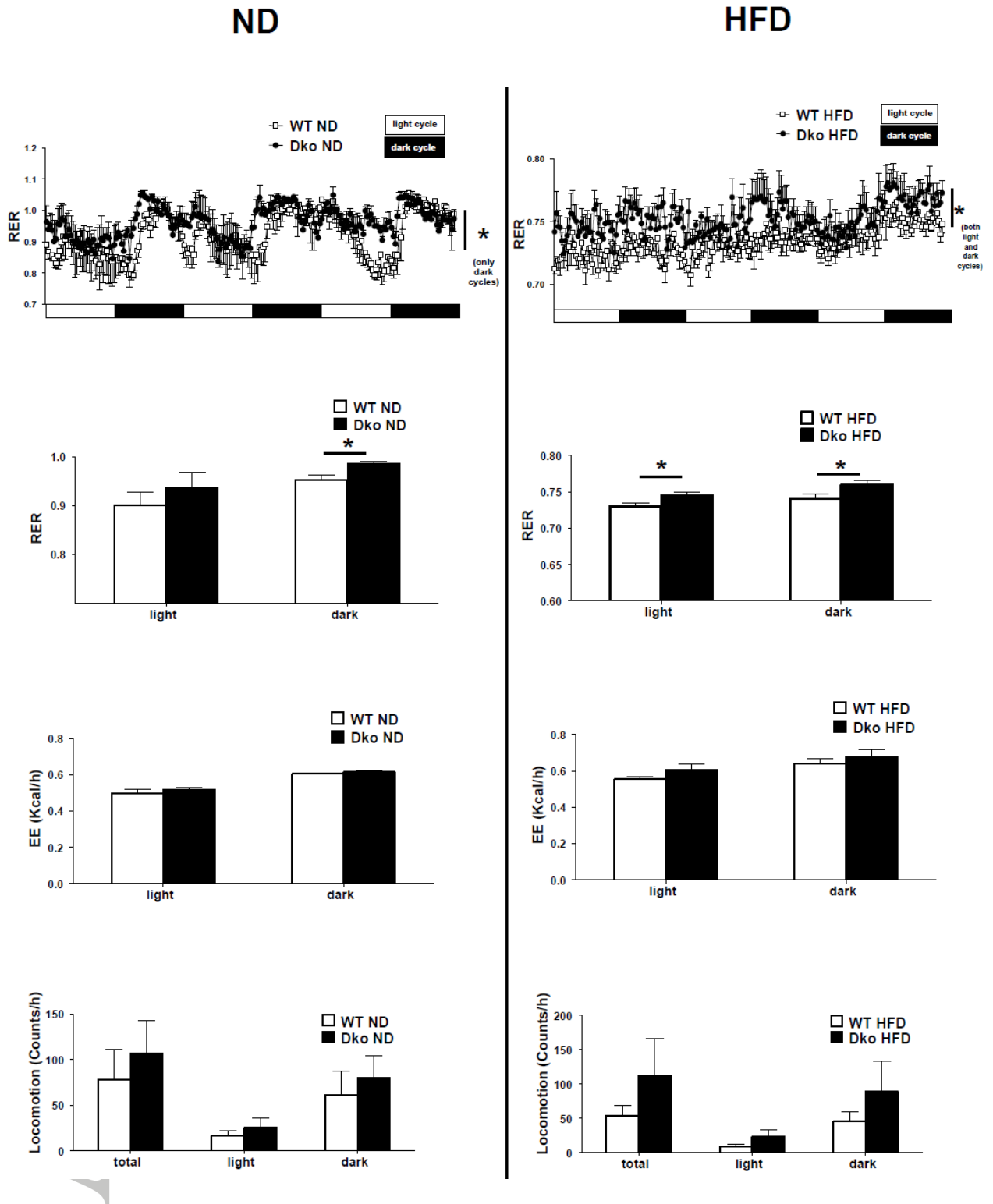
Suppl. Figure 1



Accep



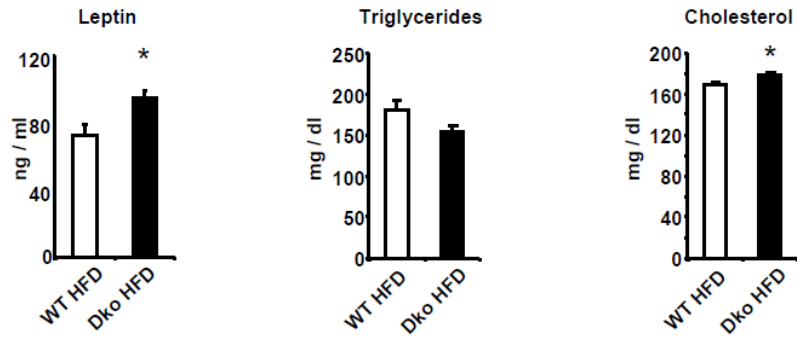
Suppl. figure 2



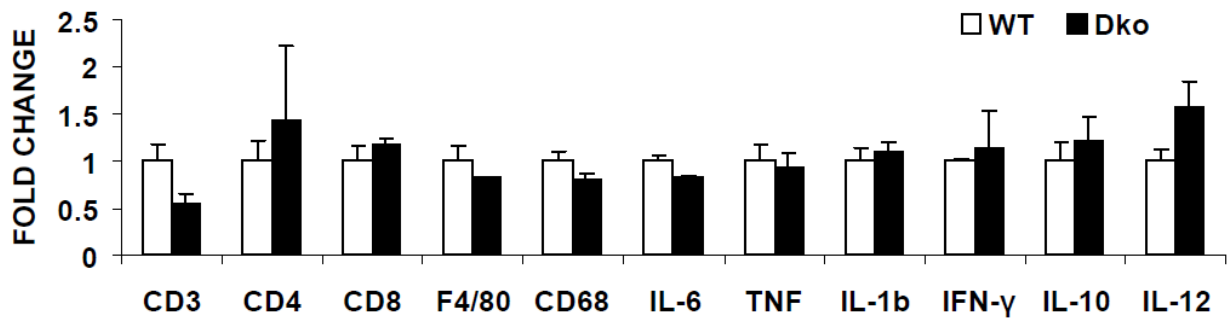


Suppl. figure 3

a



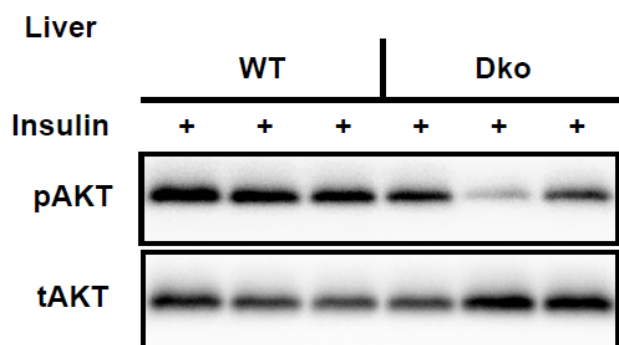
b



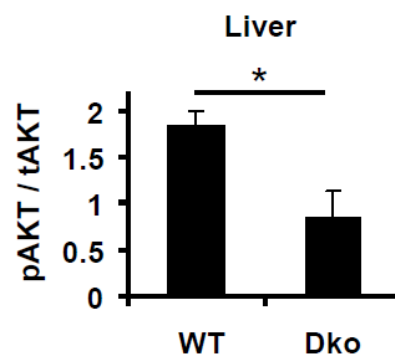
Accep


Suppl. figure 4

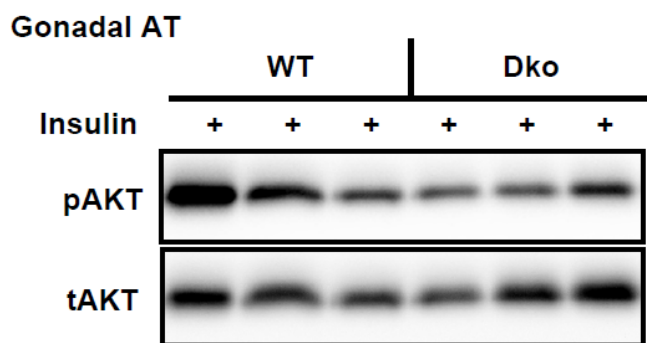
a.



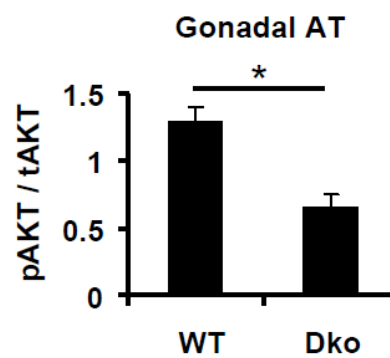
b.



c.



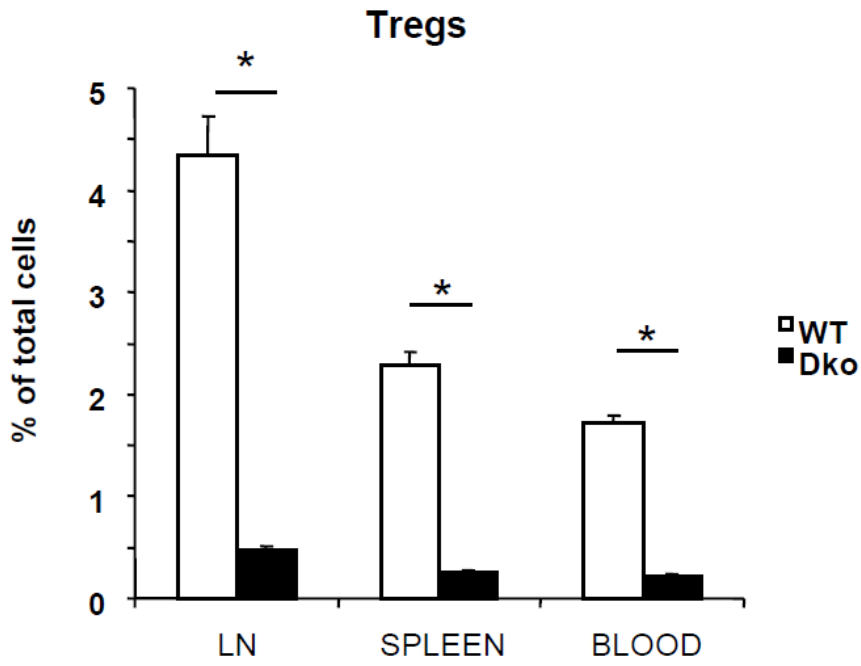
d.



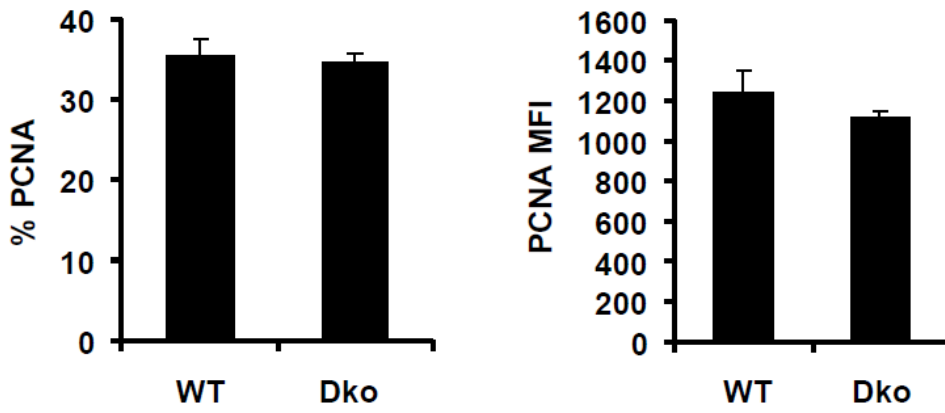
Accep

Suppl. figure 5

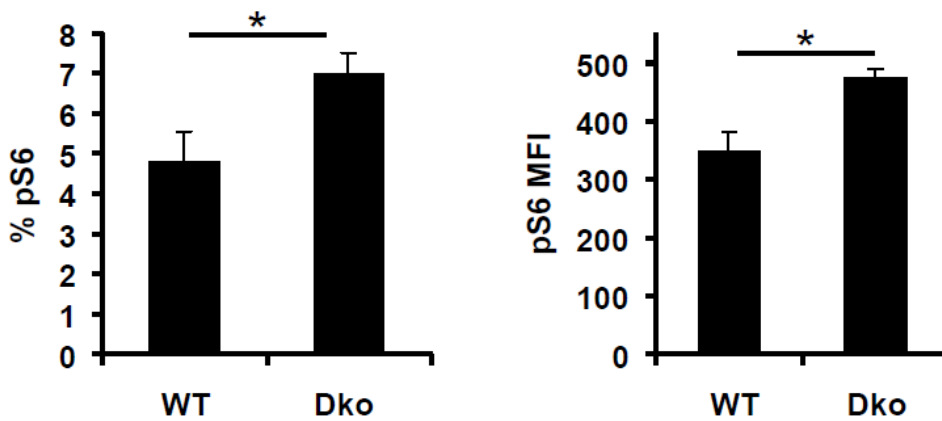
a.

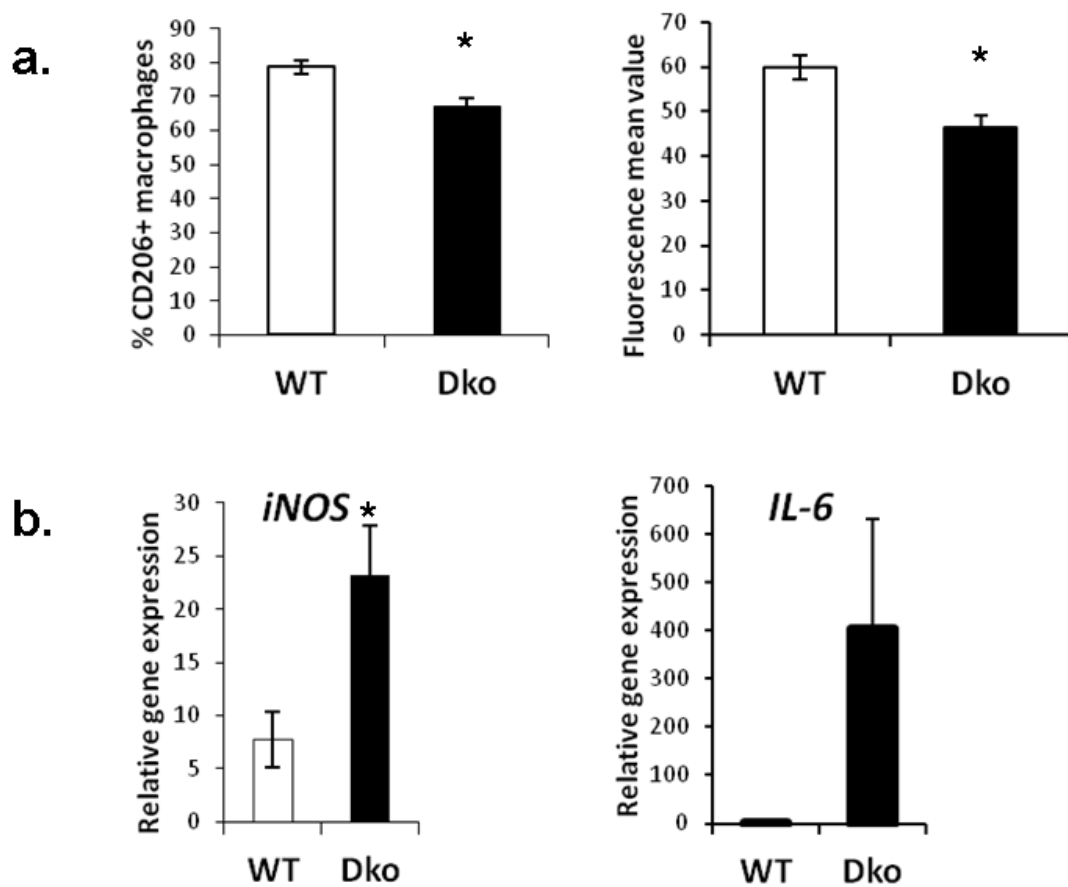


b.



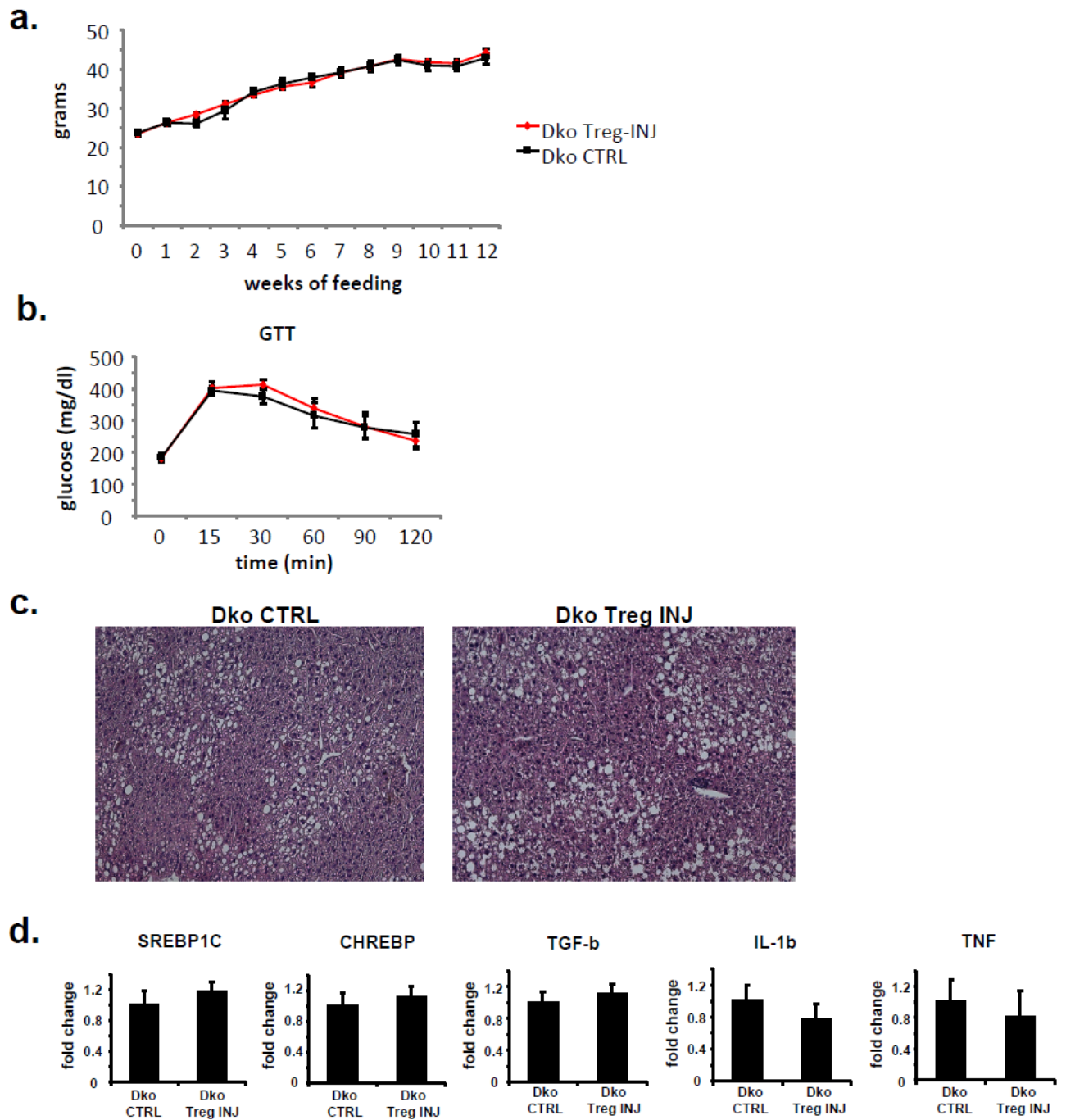
c.




Suppl. figure 6

Accep

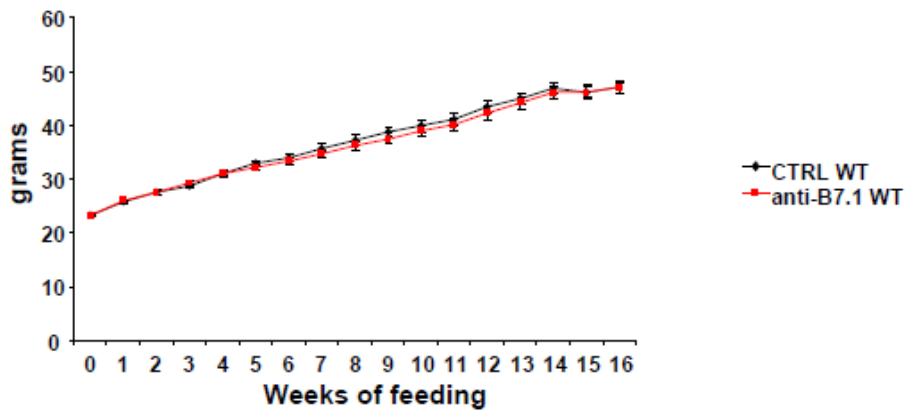
Suppl. figure 7



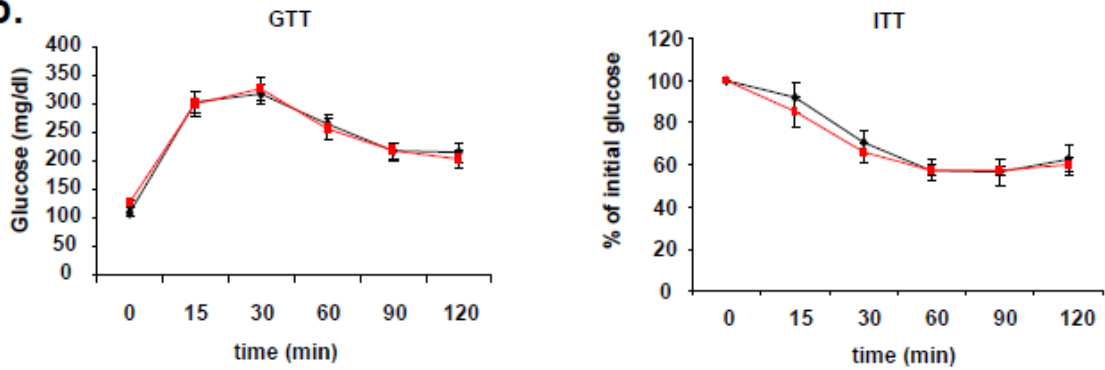


Suppl. figure 8

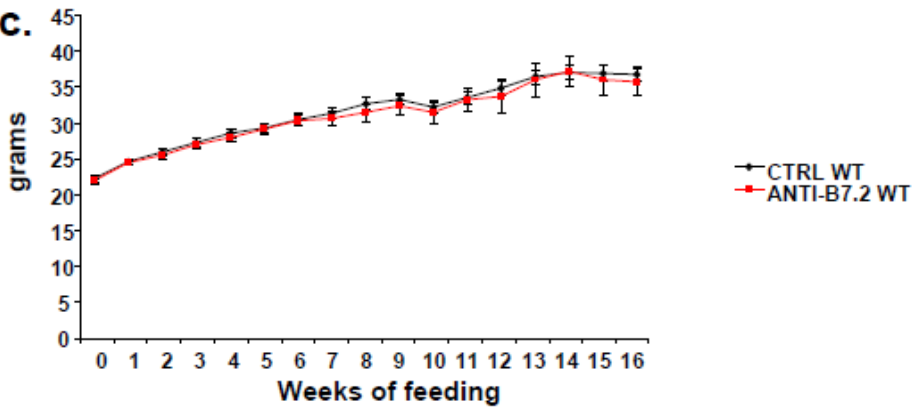
a.



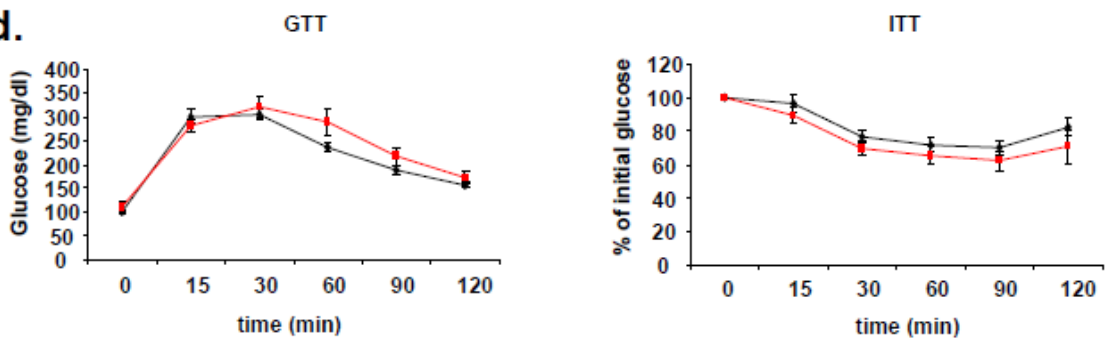
b.



c.



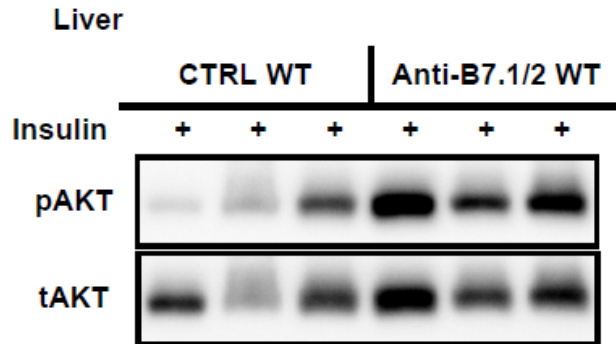
d.



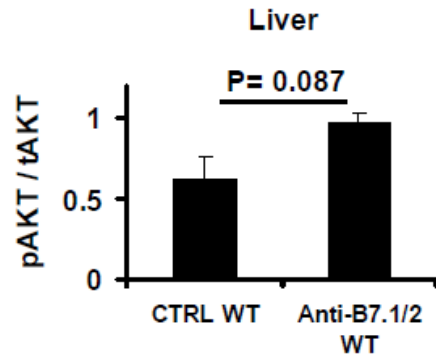


Suppl. figure 9

a.



b.

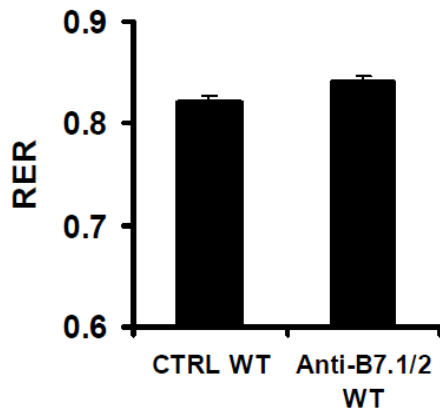


Accepted A

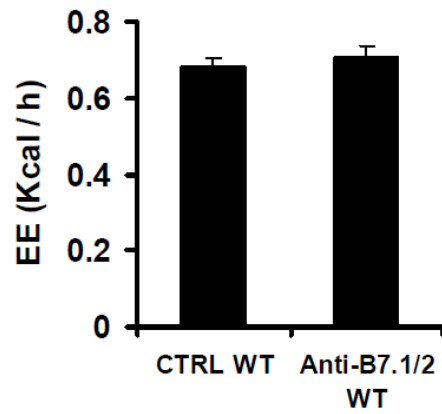


Suppl. figure 10

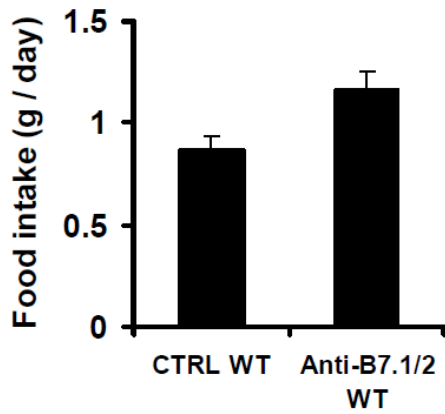
a.



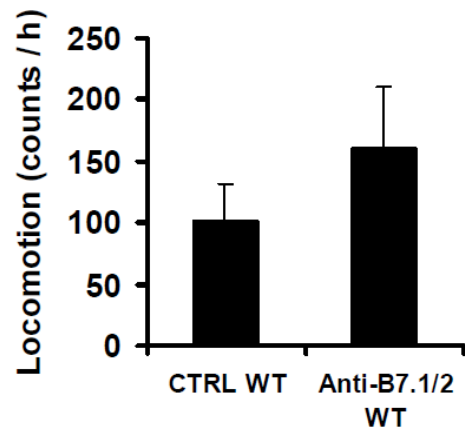
b.



c.



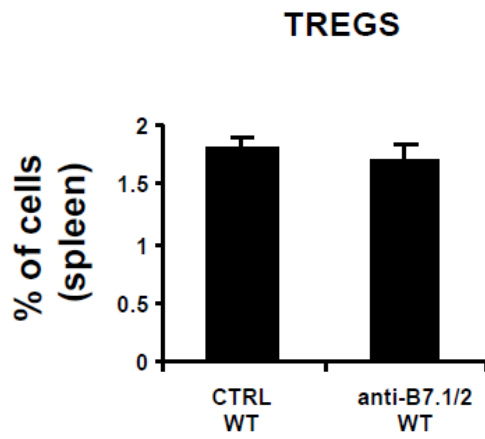
d.



ACC

cle

Suppl. figure 11



Accepte